Available online at www.sciencedirect.com

ScienceDirect

Geochimica et Cosmochimica Acta 327 (2022) 1–20

Geochimica et Cosmochimica Acta

www.elsevier.com/locate/gca

Boundary processes and neodymium cycling along the Pacific margin of West Antarctica

Ruixue Wang [a,*], Thomas J. Williams [a,b,c], Claus-Dieter Hillenbrand [b], Werner Ehrmann [d], Christina S. Larkin [a,e], Alec M. Hutchings [a], Alexander M. Piotrowski [a]

[a] Department of Earth Sciences, University of Cambridge, UK
[b] British Antarctic Survey, Cambridge, UK
[c] Institute for Marine and Antarctic Studies, University of Tasmania, Australia
[d] Institute of Geophysics and Geology, University of Leipzig, Germany
[e] The School of Ocean and Earth Science, National Oceanography Centre, University of Southampton, UK

Received 4 October 2021; accepted in revised form 12 April 2022; Available online 20 April 2022

Abstract

Neodymium (Nd) isotopes have been utilized as a tracer of water mass source in the modern ocean and in palaeoceanographic studies, though the oceanic cycling of Nd is not yet fully constrained. Recent studies have highlighted the importance of processes that occur near the seawater – sediment interface in altering the Nd isotopic composition of bottom waters. The two major observed processes "boundary exchange" and "benthic flux" have been suggested as playing an important role in setting water mass compositions, however, more studies are needed to constrain their chemical mechanism and the extent to which these processes set the composition of deep waters. The Antarctic continental margin is an important place to study these processes because Antarctic-sourced waters dominate the Southern Ocean and ventilate the global deep ocean. This study is the first to measure and compare seawater, porewater and sediment data from along the margin of Antarctica to examine the nature of potential boundary processes. We show that a process similar to boundary exchange seems to be occurring within porewaters, modifying porewater chemistry by shifting its Nd isotopic ratios to more radiogenic values without significantly increasing the concentration of dissolved Nd. We hypothesize that this shift results from partial dissolution of radiogenic detrital particles, such as smectite, amphibole and/or volcanic glass, while re-scavenging maintains low Nd concentrations. We infer the existence of benthic flux of porewaters to deep waters by examining chemical gradients in porewaters and show that it is much lower on the Antarctic margin compared to other studies. Benthic flux appears to be slightly higher along the Antarctic Peninsula than in the Bellingshausen Sea due to partial degradation of organic matter and associated dissolution of Fe-Mn oxyhydroxides. Taken together, boundary processes do not significantly change the Nd isotopic composition of Antarctic margin seawater because while the porewaters have an altered Nd isotopic composition the Nd concentration of these porewaters is low compared to other settings.
© 2022 The Authors. Published by Elsevier Ltd. This is an open access article under the CC BY-NC-ND license (http://creativecommons.org/licenses/by-nc-nd/4.0/).

Keywords: Neodymium isotopes; Neodymium cycling; Boundary exchange; Benthic flux; Antarctic margin

1. INTRODUCTION

Neodymium (Nd), one of fourteen rare earth elements (REEs), and its isotopic composition have been commonly

* Corresponding author.
E-mail address: rw581@cam.ac.uk (R. Wang).

https://doi.org/10.1016/j.gca.2022.04.012
0016-7037/© 2022 The Authors. Published by Elsevier Ltd.
This is an open access article under the CC BY-NC-ND license (http://creativecommons.org/licenses/by-nc-nd/4.0/).

used as a tracer of water mass source in the present day ocean and as a proxy for past changes in ocean circulation (e.g. Frank, 2002; Goldstein and Hemming, 2003). Neodymium isotope values are expressed as $\varepsilon_{Nd} = [(^{143}Nd/^{144}Nd)_{sample}/(^{143}Nd/^{144}Nd)_{CHUR} - 1] * 10000$ with CHUR as Chondritic Uniform Reservoir ($^{143}Nd/^{144}Nd = 0.512638$; Jacobsen and Wasserburg, 1980). The ε_{Nd} of different water masses vary due to source inputs and the short residence time of Nd relative to ocean mixing times (Tachikawa et al., 2017). This enables the reconstruction of past changes in water mass mixing and their relationship to past climate changes (e.g. Piotrowski et al., 2005; Howe et al., 2016), if this signature is preserved in authigenic marine sediment phases.

Despite the wide utilization of this proxy, two issues are still not fully understood in the modern ocean: the "Nd paradox" (Goldstein and Hemming, 2003) and the unbalanced oceanic Nd budget (Tachikawa et al., 2003). The "Nd paradox" arises from the observation that Nd isotopes appear to behave quasi-conservatively along flow paths of deep water masses, while the concentration of dissolved elemental Nd ([Nd]) in the water column profile increases with depth and thus appears to show a nutrient-like distribution (Goldstein and Hemming, 2003). Once in the ocean, dissolved Nd is likely to adsorb on particle surfaces due to the particle-reactive nature of REEs (Elderfield et al., 1988; Byrne and Kim, 1990; Scott, 1994). This scavenging preferentially causes light REEs (LREE: from La to Sm) to scavenge onto particles due to their relatively higher reactivity, leading to enrichment of heavy REEs (HREE: from Eu to Lu) in seawater. The scavenged REEs, including Nd, are subsequently released to the deeper ocean via particle dissolution and reversible exchange when particles sink down through the water column, leading to dissolved Nd concentrations that generally increase with water depth. The decoupling of [Nd] and ε_{Nd} in the ocean has been extensively discussed and generally explained by reversible scavenging in the open ocean (e.g. Siddall et al., 2008; Wang et al., 2021). The other unsolved issue arises from the estimates of the Nd budget in the modern ocean, which suggest that some of the Nd input from the solid earth is missing (Tachikawa et al., 2003). Fluvial and aeolian dust are major pathways for input of Nd (and other REEs) to the oceans (Goldstein et al., 1984; Goldstein and Jacobsen, 1987; Grousset et al., 1988, 1998; Duce et al., 1991). Other possible sources include hydrothermal Nd flux, which, however, has been shown to be a net sink (Elderfield et al., 1988, and references therein; Stichel et al., 2018), and submarine groundwater discharge (Johannesson and Burdige, 2007), which cannot be reliably quantified due to a lack of data.

The input of Nd (and other REEs) from seabed sediments into the ocean through the water - sediment interface is also important and can help to resolve the two issues. Here we refer to all processes occurring at the water - sediment interface and within the uppermost layer of the seabed (about 0–40 cm depth) as "boundary processes". There are generally two types of processes, "benthic flux" and "boundary exchange", that have been extensively investigated. Benthic flux can modify both [Nd] and ε_{Nd} of local bottom water (Abbott et al., 2015a) as porewaters with a high concentration of dissolved Nd diffuse upwards in sediment porewater into bottom waters. The ε_{Nd} of the porewaters are different from bottom waters due to Nd release from desorption from particles, reduction of authigenic phases or dissolving detrital particles. This has been observed on the California margin (Haley et al., 2004), in Buzzards Bay (Massachusetts continental shelf; Sholkovitz et al., 1989), on the Oregon continental slope (Abbott et al., 2015b), and on the Australian continental margin in the Tasman Sea (Abbott, 2019). Boundary exchange is defined as the transfer of elements from the seabed sediments into the seawater by particle dissolution, accompanied by the simultaneous removal of elements from the seawater by boundary scavenging (Lacan and Jeandel, 2005; Arsouze et al., 2009). It can cause a modification of ε_{Nd} in bottom water without causing a significant change in [Nd]. The exact mechanism of this Nd modification, however, remains unconstrained. Both boundary processes may be important for solving the oceanic Nd budget problem and the "Nd paradox", especially along continental margins, where these processes are most likely to occur. Therefore, to better understand their importance for potentially altering the Nd signal of global ocean circulation, it is necessary to jointly investigate the Nd compositions of bottom waters, porewaters, authigenic Fe-Mn oxyhydroxide coatings of marine sediment particles and the detrital fraction on continental margins.

The Antarctic continental margin is an important location to investigate the processes setting the REE and Nd isotope fingerprints of deep- and bottom water masses. This is because water masses in the Southern Ocean mix with waters from the Atlantic, Indian and Pacific Oceans. Additionally, Antarctic Bottom Water (AABW), a key water mass in the global thermohaline circulation, forms at various locations along the continental margin of Antarctica (e.g., Meredith, 2013). The complex geology of the Antarctic continent, especially the contrasts between East and West Antarctica, leads to a large variation in the ε_{Nd} of detrital particles to the surrounding margin (Roy et al., 2007; Simoes Pereira et al., 2018; Wilson et al., 2018). Freshly eroded detrital particles with a large span of ε_{Nd} compositions potentially affect the composition of waters along the Antarctic margin and hamper palaeoreconstructions of ocean circulation using ε_{Nd}. Carter et al. (2012), Rickli et al. (2014) and Basak et al., 2015 analysed ε_{Nd} and [Nd] of the water column in various locations along the Antarctic continental shelf and rise, focusing on the Ross, Amundsen, and Bellingshausen Seas. The data suggest ε_{Nd} modification of bottom waters towards more radiogenic values via boundary processes, with [Nd] also being altered at one sampling site on the Marie Byrd Seamounts in the Amundsen Sea (Rickli et al., 2014). To unravel the mechanisms of possible modification of ε_{Nd} and [Nd] of deep- and bottom-water masses, direct studies from the seawater – seafloor interface are required. Here we present results from a combined Nd water column, porewater and seabed sediment study on the West Antarctic continental margin in order to characterize the boundary processes affecting ε_{Nd} and [Nd] in this region.

1.1. Study area

The three studied sites are located on the West Antarctic continental rise west of the Antarctic Peninsula and in the Bellingshausen Sea (Fig. 1 and Table 1). Circumpolar Deep Water (CDW) occupies most of the water column under the colder, but fresher Antarctic Surface Water (AASW). The bottom water flowing southwest along the slope and on the upper continental rise west of the Antarctic Peninsula is colder, fresher and more oxygenated than CDW. This contour current is thought to comprise modified Weddell Sea Deep Water (WSDW). The WSDW flows out of the Weddell Sea through deep gaps in the South Scotia Ridge, turns westward around the northern tip of the Antarctic Peninsula and thereby is modified by mixing with overlying Lower Circumpolar Deep Water (LCDW), which also originates from the Weddell Sea (Camerlenghi et al., 1997; Giorgetti et al., 2003; Hillenbrand et al., 2008a; Hernández-Molina et al., 2017).

The cores in this study were taken from the upper continental rise west of the Antarctic Peninsula, where there is a series of large asymmetrical-shaped mounds interpreted as sediment drifts (e.g. Hernández-Molina et al., 2017; Rebesco et al., 1997), whose depositional regime is controlled by the southwestward-directed bottom-water flow and its interaction with downslope turbidity currents (e.g. Pudsey, 2000; Rebesco et al., 1996, 2002). The mounds are 100–300 km long, oriented perpendicular to the continental margin, 50–100 km wide and elevated several hundred meters above adjacent channels that were eroded by turbidity currents (Rebesco et al., 1997, 2002). The uppermost parts of the drifts are formed by Late Quaternary sediments consisting of brown, biogenic, bioturbated muds with ice-rafted debris (IRD) deposited during interglacials and grey, terrigenous, laminated muds deposited during glacials (Pudsey and Camerlenghi, 1998; Pudsey, 2000; Lucchi et al., 2002). Sedimentation rates vary from ~1–20 cm/kyr, are usually several cm/kyr, and often are higher during a glacial period (Pudsey and Camerlenghi, 1998; Pudsey, 2000; Lucchi et al., 2002; Hillenbrand et al., 2021). Our study area also includes a huge drift located on the continental rise of the western Bellingshausen Sea at 94°W (Nitsche et al., 2000; Cunningham et al., 2002) with an asymmetric shape which suggests a continuation of westward bottom-current flow to at least 94°W (Hillenbrand et al., 2003). Its Late Quaternary sediments resemble those of the drifts along the Antarctic Peninsula (Hillenbrand et al., 2021).

Between the continental rise drifts offshore from the Antarctic Peninsula and in the western Bellingshausen Sea the Belgica Trough Mouth Fan forms the largest depocenter (Scheuer et al., 2006; Dowdeswell et al., 2008) (Fig. 1). The fan received glacigenic detritus supplied through Belgica Trough, a prominent bathymetric trough on the southern Bellingshausen Sea shelf, which was eroded and occupied by a palaeo-ice stream during past glacial periods (Ó Cofaigh et al., 2005; Hillenbrand et al., 2010). The ice stream was fed by an interior ice-sheet basin that exceeded

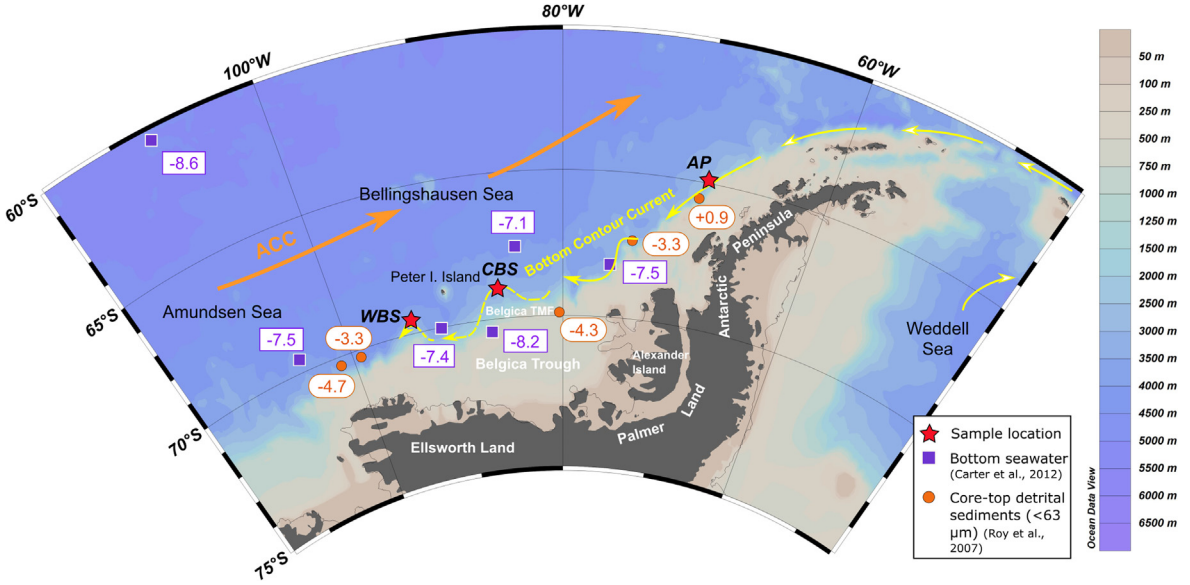

Fig. 1. Bathymetric map of the study area with locations of investigated sites, major bottom currents and deep-water mass flow along the western Antarctic Peninsula (AP) and in the Bellingshausen Sea (CBS: central Bellingshausen Sea, WBS: western Bellingshausen Sea; Belgica TMF: Belgica Trough Mouth Fan). Orange arrows mark Antarctic Circumpolar Current (ACC) flow of Circumpolar Deep Water (CDW), and yellow arrows denote bottom contour current flow of waters originating from the Weddell Sea along the continental rise, with continuous arrows marking measured flow and dashed arrows marking inferred flow (Camerlenghi et al., 1997; Giorgetti et al., 2003; Hillenbrand et al., 2003; Hillenbrand et al., 2008a). Nd isotopic compositions of nearby bottom water (Carter et al., 2012) and core-top detrital sediment (Roy et al., 2007) are shown by purple squares and orange circles, respectively.

Table 1
Locations of study sites and deployed gear.

Site ID	CTD ID	Giant Box Core (GBC) ID	Latitude (^{o} S)	Longitude (^{o} W)	Water depth (m)	Subcore recovery (cm)
AP	PEN_1	722	64^{o} 53.72′	69^{o} 02.14′	2329	32
CBS	BELS_1	724	68^{o} 56.57′	85^{o} 47.40′	3073	40
WBS	BELS_2c	725	69^{o} 31.90′	93^{o} 54.95′	3660	41

an area of 200,000 km^2 and included parts of southern Alexander Island, south-western Palmer Land and the Bryan Coast of Ellsworth Land (Ó Cofaigh et al., 2005; Dowdeswell et al., 2008) therefore supplying sediments with a wide range of lithology, mineralogy, and geochemistry. The drainage area of the Belgica palaeo-ice stream is only constrained by a few marine sediment cores, but probably changed through time according to the clay mineralogical heterogeneity of subglacial tills and glacigenic debris flows recovered from the shelf and the trough-mouth fan (Hillenbrand et al., 2005, 2009).

2. MATERIAL AND METHODS

2.1. Sampling

Seawater, porewater and sediment samples were collected from three sites during cruise JR298 of the RRS *James Clark Ross* in 2015. Porewater and sediment samples were firstly collected in a Giant Box Corer (GBC) and separated later in the lab. The locations of the three study sites are listed in Table 1 and shown in Fig. 1. The water column above each GBC site was sampled with a CTD cast. For accessibility, in this paper we use for CTDs and GBCs deployed at the same site IDs according to their locations: site AP (Antarctic Peninsula), site CBS (central Bellingshausen Sea), and site WBS (western Bellingshausen Sea) (see Table 1).

Seawater samples were drawn from Niskin bottles mounted on a CTD rosette. Seawater samples for trace metal concentration analyses were filtered through 0.45 μm AcroPak Supor® filters and then stored in 125 ml acid-cleaned plastic Nalgene bottles. Bottom water samples for [Nd] and ε_{Nd} analyses were collected in 10 L acid-cleaned polyethylene bottles. All trace metal and Nd isotope samples were subsequently acidified to pH ~2.5 with single distilled HCl. The samples were stored in a refrigerator before being analysed.

Three GBCs (dimensions: 50 cm × 50 cm, 60 cm depth) were collected. When a GBC landed on deck after recovery, about 2 L of seawater were sampled from above the sediment surface by syphoning it off without disturbing the seafloor surface sediments. These samples are assumed to be a mixture of bottom seawater and surface sediment pore water. They are referred to in this paper as "interface water". Then the water samples were filtered and acidified to pH ~2.5 with single distilled HCl in acid-cleaned plastic Nalgene bottles. The samples were stored in a fridge at + 4 °C before being used.

Sub-cores were taken from each GBC on deck. Three sub-cores (diameter 10 cm) from each box core were sampled in a sediment core processing laboratory onboard. The sub-cores were extruded from the core liners in 1 cm intervals and cut into 1 cm-thick slices with a ceramic knife. The cores were entirely sampled in this manner from the sediment water interface to their base. The sediment slices were immediately transferred into individual vacuum sealed bags and stored frozen to minimize contact with ambient air and oxidation of reduced species in potentially sub-oxic intervals of the cores. The exposure time of each sample was less than 2 hours. According to the Einstein–Smoluchowski relation, diffusion will carry solutes, such as O_2, only over a distance of 3 mm in 2 h (Paul et al., 2019). Therefore, our sampling after sub-coring was quick enough to avoid changes in the dissolved signal due to oxidation, (Schnetger and Dellwig, 2012).

All geochemical analyses took place in the laboratories of the Department of Earth Sciences, University of Cambridge, UK. The sediment samples were defrosted in an anaerobic chamber and then transferred into 50 ml acid-cleaned centrifuge tubes. The tubes were sealed and centrifuged at 4500 rpm for 20 minutes. The tubes were then transferred back to the anaerobic chamber for porewater collection. Around 30 to 100 ml of porewater were extracted depending on the porosity in different depths. The porewater samples were transferred with an acid-cleaned syringe through 0.2 μm filters into acid-cleaned centrifuge tubes and acidified to pH ~ 2.5. The residues were then dried at 50 °C in an oven.

Post-cruise analyses on other sediment cores from the studied GBC sites showed that the average sedimentation rates for Marine Isotope Stage 1 (MIS 1; 0–14 ka) at these sites are ≥ 4.3 cm/kyr, suggesting that all of our samples are younger than ~10 ka (Channell et al., 2019; Hillenbrand et al., 2021). For detailed information on the sediments recovered in the analysed GBCs the reader is referred to Hillenbrand et al. (2021) and the related datasets archived under https://doi.pangaea.de/https://doi.org/10.1594/PANGAEA.927866.

2.2. Analytical procedures

2.2.1. REEs and Nd isotopes

2.2.1.1. Sample preparation. The concentration of REEs in seawater and porewater samples was measured by using the isotope dilution (ID) method improved from Greaves et al. (1989), Rickli et al. (2009), and Rousseau et al. (2013). About 50 g seawater sample (10 g for porewater) were weighed in acid cleaned centrifuge tubes and spiked with 0.2 g multi-REEs spike (the spike follows Greaves et al., 1989). After overnight equilibration, 1 mg iron (in cleaned $FeCl_3$ solution) was added to the samples, and the tubes were vigorously shaken. After a few hours equilibration, iron hydroxide flocculation ($Fe(OH)_3$) was induced by

raising the pH to 7.5 ± 0.5 by addition of NH_4OH. The precipitate was centrifuged after overnight settling and the supernatant was carefully decanted by pipette. The precipitate was rinsed with 25 ml MQ water and centrifuged twice in order to remove soluble salts (e.g. NaCl), and then transferred in a few ml of MQ water into 15 ml Teflon vials. After drying, the samples were heated on a hot plate in 0.66 ml of aqua regia for 24 h to oxidize organic compounds. Then the samples were dried on a hot plate and re-dissolved in 0.25 ml of 6 M HCl twice to convert them into the chloride-form.

For Nd isotope analysis of seawater (~10 L) and "interface water" (~2 L) samples, the same pre-treatment as above was applied but 50 mg iron and no spike was added. For detrital sediments, the <63 μm fraction was obtained by wet sieving of the samples. After drying, this fine fraction was treated with sequential leaching to remove carbonate by 0.44 M acetic acid buffered to pH 5 by sodium acetate, and to remove Fe-Mn oxyhydroxides by 0.02 M hydroxylamine hydrochloride (HH) in 25% acetic acid (v/v) following the procedure of Li (2018). Around 30 mg for each leached sample was taken and treated with 2 ml 5% H_2O_2 at room temperature for 24 hours to oxidise organic carbon. After drying, the samples were dissolved in a mixture of 1 ml 16 M HNO_3 and 0.5 ml 47% HF at 110 °C in Teflon vials on a hotplate for 48 hours. After renewed drying, the samples were dissolved in 1.5 ml aqua regia (16 M HNO_3 and 10 M HCl at 1:3 molar ratio) at 80 °C for another 24 hours to further destroy the remaining organic matter and dried again.

The ε_{Nd} composition of porewaters could not be analysed directly due to relatively low Nd concentrations and lack of sufficient sample volume. Instead, we measured the Nd isotopic composition of acid-reductive leachates which have been designed to liberate Fe-Mn oxyhydroxide coatings without attacking detrital sediment phases. We discuss the validity of our approach further in Section 4.1. Approximately 1.8 g bulk or fine-grained (<63 μm) sediment, depending on the sample availability, was treated with ~10 ml 0.005 M Hydroxylamine-Hydrochloride (HH) leachates (with EDTA and acetic acid at buffered pH = 4) for ~1 h following the protocol of Blaser et al. (2016). Recently, Huang et al. (2021) has improved this method by applying a shorter leaching time. However, a method comparison using our samples showed no differences between the results obtained from the bulk and fine fractions, or whether the Blaser and Huang method was applied (supplementary text 1, Fig. A1). Therefore, we treated samples following Blaser et al. (2016) on bulk and fine fraction sediments. The leachates were centrifuged and dried before being redissolved in 2 ml of aqua regia at 80 °C for 24 h in order to oxidize organic compounds; they were then dried again before column chromatography.

2.2.1.2. Column chromatography. REEs were separated from sample matrix ions, especially Fe and Ba, through cation exchange column chemistry following procedures modified from Greaves et al. (1989). The columns used had a diameter of 3 mm and a height of 3.7 cm with a resin bed (AG50W-X8, 200–400 mesh) of 0.26 ml volume.

For Nd isotope analysis, water samples first had REE separated from Fe using a cation exchange column method (Larkin et al. (2021) modified from Dausmann (2018)). The columns used had a diameter of 1.5 cm and a height of 11.3 cm with a resin bed (AG50W-X8, 200 to 400 mesh size) of 20 ml volume. The REEs were further purified by another cation exchange column following the same procedures as described above for obtaining REE concentrations. Finally, Nd was separated from the other REEs using Eichrom LNspec^{TM} resin (50–100 μm mesh) on volumetrically calibrated columns. For detrital sediment and leachate samples, REEs were separated using Eichrom TRUspec^{TM} resin, and Nd was then separated from the other REEs by Eichrom LNspec^{TM} resin using volumetrically calibrated columns.

2.2.1.3. Measurements. REE multispike ID measurements were performed by ICP-MS (Element-XR, Thermo-Fisher Scientific) at the Department of Earth Sciences, University of Cambridge. The ICP-MS was operated in low resolution mode with a quartz APEX-IR introduction system with added N_2 following Larkin et al. (2021), a method modified from Greaves et al. (1989) and Rousseau et al. (2013). Oxide generation was monitored and minimised by optimising inject rates of the gases, with oxide and isobaric interferences corrected for offline. Blanks and reproducibility are listed in the supplementary text 2.

Nd isotopes were measured on a Thermo Scientific Neptune Plus MC-ICP-MS at the Department of Earth Sciences, University of Cambridge. The mass fractionation was corrected by normalizing $^{146}Nd/^{144}Nd$ to 0.7219 using an exponential correction. Each sample was bracketed with analyses of the JNdi-1 neodymium isotopic standard with a $^{143}Nd/^{144}Nd$ value corrected to 0.512115 ± 7 as reported by Tanaka et al. (2000). A sample from the Bermuda Atlantic Time Series Station BATS (15 m depth) was used as an independent external reference standard (Wang et al., 2021). Blanks were always representing <1% of the final sample size of water sample, and <0.1% of leachate or detritus sample. The uncertainties were calculated from 2 times of standard deviation (2SD) of JNdi-1 in a whole run. Details of blanks and long-term reproducibility are listed in the supplementary text 3.

2.2.2. Other trace and major metal elements

Concentrations of other trace elements (Fe, Mn and U) in porewaters were measured on ICP-MS (Element-XR, Thermo-Fisher Scientific) with 100-fold dilutions at the Department of Earth Sciences, University of Cambridge. The measurements used a matrix-matched calibration line, with a Na concentration of ~100 ppm, made from single element standards. Fe and Mn were measured in medium resolution mode, and the instrument was tuned to deconvolve the ^{56}Fe peak from the $^{40}Ar^{16}O$ peak. The detection limits for Fe and Mn concentrations are 0.3 nM and 0.5 nM, respectively. Uranium was measured in low resolution mode. Instrumental drift was corrected for by repeated measurements of an internal standard. The uncertainties for Fe, Mn, and U concentration are 6.1%, 6.3%, and 5.6% respectively.

Leachates were analysed for Al and Nd concentrations by ICP-OES (Agilent 5100) following Larkin et al. (2021), with a reproducibility better than 10%.

2.2.3. Clay mineral analyses

In order to provide further constraint on sediment source and reactivity in porewaters, clay mineral assemblages were investigated on discrete down-core samples from the GBCs using X-ray diffraction (XRD) methods at the Institute of Geophysics and Geology, University of Leipzig. The clay fraction (<2 μm) was separated from the bulk sediment by settling, and 40 mg of clay was dispersed in an ultrasonic bath and mixed with 1 mL of an internal standard consisting of a 1% MoS_2 suspension. The XRD measurements followed standard procedures and methods previously published in Ehrmann et al. (1992, 2011), Petschick et al. (1996) and Hillenbrand et al. (2009).

3. RESULTS

3.1. Nd concentrations and Nd isotopic compositions

In the seawater column, dissolved neodymium concentration ($[Nd]_d^{sw}$) generally increases with depth from 13.0 to 28.5 pmol/kg (Fig. 2, Table S1), with an obvious increase in bottom water concentrations at site AP. The deepest samples were taken at 6 m above seafloor at site AP, at 10 m above seafloor at site CBS, and at 5 m above seafloor at site WBS. Dissolved Nd isotopic composition of bottom water ($\varepsilon_{Nd\ d}^{bw}$) of around −7.5 is uniform within the analytical uncertainty at the three sites (2SD = 0.38). At site AP, $\varepsilon_{Nd\ d}^{sw}$ ranges from −7.8 to −8.8 through the water column, with the sample from intermediate water depth (880 m) having the least radiogenic value (Fig. 2, Table S3).

Within porewaters, concentrations of dissolved Nd ($[Nd]_d^{pw}$) are generally higher than within the seawater, and vary at different sub-bottom depths (Fig. 2, Table S2). $[Nd]_d^{pw}$ profiles are similar at sites CBS and WBS, where $[Nd]_d^{pw}$ near the seafloor surface (depth 0–10 cm) is slightly higher than in the bottom water and increases with sub-bottom depth up to 130.4 pmol/kg (depth > 10 cm). At site AP $[Nd]_d^{pw}$ reaches 111.8 pmol/kg in the uppermost layer of sediment and, thus, is much higher than in the bottom water (28.0 pmol/kg). $[Nd]_d^{pw}$ varies significantly down-core, without falling below the bottom water concentration, but shows no clear down-core trend. Concentrations of other dissolved REEs, except cerium (Ce), have similar variation trends to Nd with sediment depth (Fig. 3, Table S2).

Nd isotopic ratio of authigenic Fe-Mn oxyhydroxide coatings extracted by HH leaching (ε_{NdHH}) ranges from −6.2 to +0.5 and increases down-core at all three sites, with a strong increase observed at shallow sub-bottom depths above ~10 to 15 cm and very minor changes below (Fig. 2, Table S3). Nd isotopic compositions of fine-grained detrital sediments (ε_{Ndsed}) range from −2.7 to −4.4 and −1.1 to −5.9 at sites CBS and WBS, respectively, displaying a slight decrease with sediment depth in the upper ~15 cm and constant ε_{Ndsed} below (Fig. 2, Table S3). ε_{Ndsed} at site AP is about 0.0 and does not vary down-core within the analytical error (2SD = 0.23).

The "interface water" from sites AP and WBS has Nd concentrations ($[Nd]_d^{iw}$) close to those of the bottom water at these sites. Its ε_{Nd} values (ε_{Nd} *diw*) fall between ε_{Nd} *dsw* of the bottom water and ε_{NdHH} of Fe-Mn oxide fraction of the seafloor surface sediments (Fig. 2, Table S2 and S3).

3.2. Other trace metals

Dissolved iron concentrations of porewater and bottom water ($[Fe]_d^{pw}$ and $[Fe]_d^{bw}$) are mostly below the detection limit (0.3 nM) at sites CBS and WBS, while reaching 1.1 μM at 21–22 cm depth at site AP (Fig. 3). Similarly, dissolved manganese concentrations ($[Mn]_d^{pw}$ and $[Mn]_d^{bw}$) are elevated at site AP, where concentrations reach up to 0.09 μM, while being mostly below the detection limit (0.5 nM) at the other two sites (Fig. 3). The dissolved uranium concentrations of bottom water ($[U]_d^{bw}$) at all three sites and of interface water ($[U]_d^{iw}$) at site AP are similar, ranging from 11.6 to 12.6 nM (Fig. 3, Table S5). The uranium concentration within porewater ($[U]_d^{pw}$) is mostly lower than in the overlying waters, ranging from 2.8 to 12.6 nM, and generally decreases with sediment depth. The uranium concentration of the "interface water" ($[U]_d^{iw}$) was only measured at site AP due to lack of sufficient sample residue at site WBS.

3.3. Clay mineral assemblages

The clay mineral distribution of the down-core sediments is shown in Fig. 4 and given in Table S6. Smectite, illite, chlorite, and kaolinite account for 13–30%, 30–53%, 25–41%, and 1–8% of the clay mineral composition, respectively. Smectite decreases down-core at all sites, with the most prominent decrease observed in the upper ~20 cm at sites WBS and CBS, which mirrors the down-core decrease in ε_{Ndsed} at these sites (Fig. 4). In general, the proportions of illite and kaolinite increase on the expense of smectite and chlorite in a westward direction from site AP via site CBS to site WBS.

4. DISCUSSION

4.1. Nd isotopic composition of porewater

The ε_{Nd} composition of leachates reflect the composition of authigenic Fe-Mn oxides, which formed from seawater, but also may contain a signature from porewater processes. In palaeoceanographic studies the core-top leachate is often compared to modern bottom water ε_{Nd} values to test whether the ε_{Nd} value of seawater was preserved by the Fe-Mn oxides or was subsequently overprinted during early diagenesis by processes occurring in the porewaters (e.g. Piotrowski et al., 2005; Howe et al., 2016). In our study, the core-top ε_{NdHH} values at all sites are offset to more radiogenic values than the ε_{Nd} *dsw* of the bottom water (Fig. 2),

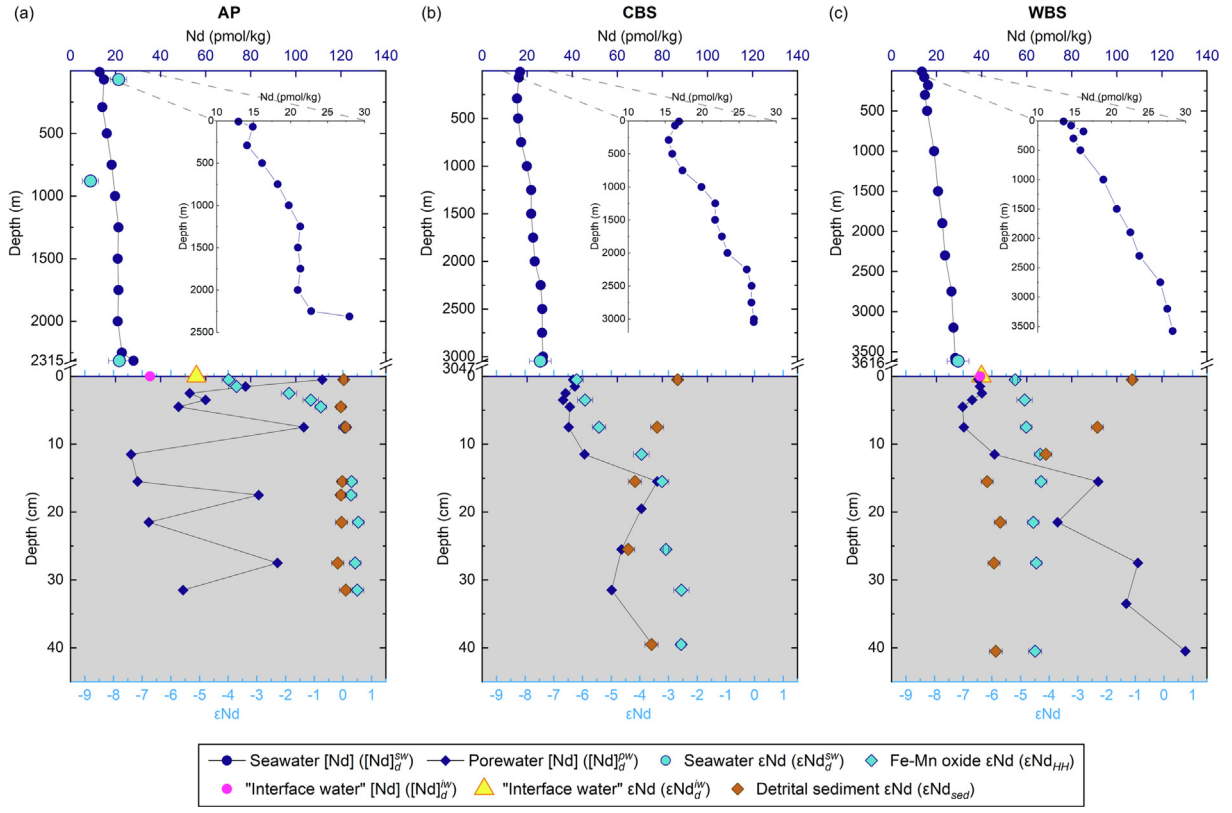

Fig. 2. Nd concentrations and Nd compositions of combined seawater, porewater and fine-grained detrital sediments at the studied sites (a) AP, (b) CBS, and (c) WBS. The εNd composition of porewater could not be measured directly but is inferred from the εNd composition of authigenic Fe-Mn coatings. The inset figure at each site shows the seawater Nd concentration profiles on an enlarged scale.

and therefore must have been affected by diagenetic or boundary processes.

We exclude the possibility that the leachates were changed by dissolution of detrital sediments during leaching in the laboratory because a comparison of different leaching methods (see supplementary text 1) yielded the same isotopic composition, and all the leaching tests had a low Al/Nd ratio of <60, i.e., lower than the threshold mass ratio of 100 suggested for good quality Nd isotope data by Huang et al. (2021). If a significant amount of detritus was dissolved during leaching, the amount of lithogenic Nd and Al released to the solution could be expected to vary with HH leaching time (Wilson et al., 2013). Instead, we interpret the more radiogenic signature of the leachates to reflect that of the porewaters. Further evidence for this is that the "interface water" which was sampled from the box core has an ε_{Nd} value in between that of bottom water and the core-top HH leachate (Fig. 2). This is consistent with the more radiogenic porewaters mixing with bottom waters. Therefore, we interpret the HH leachates as being derived from Fe-Mn oxyhydroxides which precipitated and captured the porewater ε_{Nd} during the diagenetic process in the upper layer of the marine sediments (Bau et al., 1996), that the porewaters ε_{Nd} is likely to be more radiogenic than modern seawater, and that the down-core ε_{NdHH} profiles are largely likely reflecting porewater compositions rather than past seawater variations.

4.2. Redox environment

Dissolved U is conservative at around 3.3 ppb (or 13.9 nM) in oxygenated seawater (Ku et al., 1977) and decreases in suboxic and anoxic porewater because soluble U (VI) reduces to insoluble U (IV) (Klinkhammer and Palmer, 1991). At our study sites, U concentration of bottom water is 11.5 - 12.6 nM, close to the conservative value, while in porewater it generally decreases with sediment depth but is always above 0 (Fig. 3). The slightly lower [U] of bottom water than the conservative value likely results from oxygen consumption by organic matter decomposition at the seafloor (Hammond et al., 1996). The [U] profiles in the sediment cores indicate that all our samples are from an oxic porewater environment and the redox boundary lies below the maximum GBC penetration depth. This interpretation is consistent with observations of the down-core extent of both solid-phase Mn enrichments and the authigenic magnetic mineral maghemite, which forms by surface oxidation and is dissolved below the oxic zone, in long piston cores recovered from the same study sites (Channell et al., 2019; Hillenbrand et al., 2021). An oxic porewater environment for our samples is also supported by the fact that in most of our analysed porewaters the concentrations of Fe and Mn are either below or just above the detection limits (Shaw et al., 1990). We suggest that the observed down-core [U] gradient in the porewaters

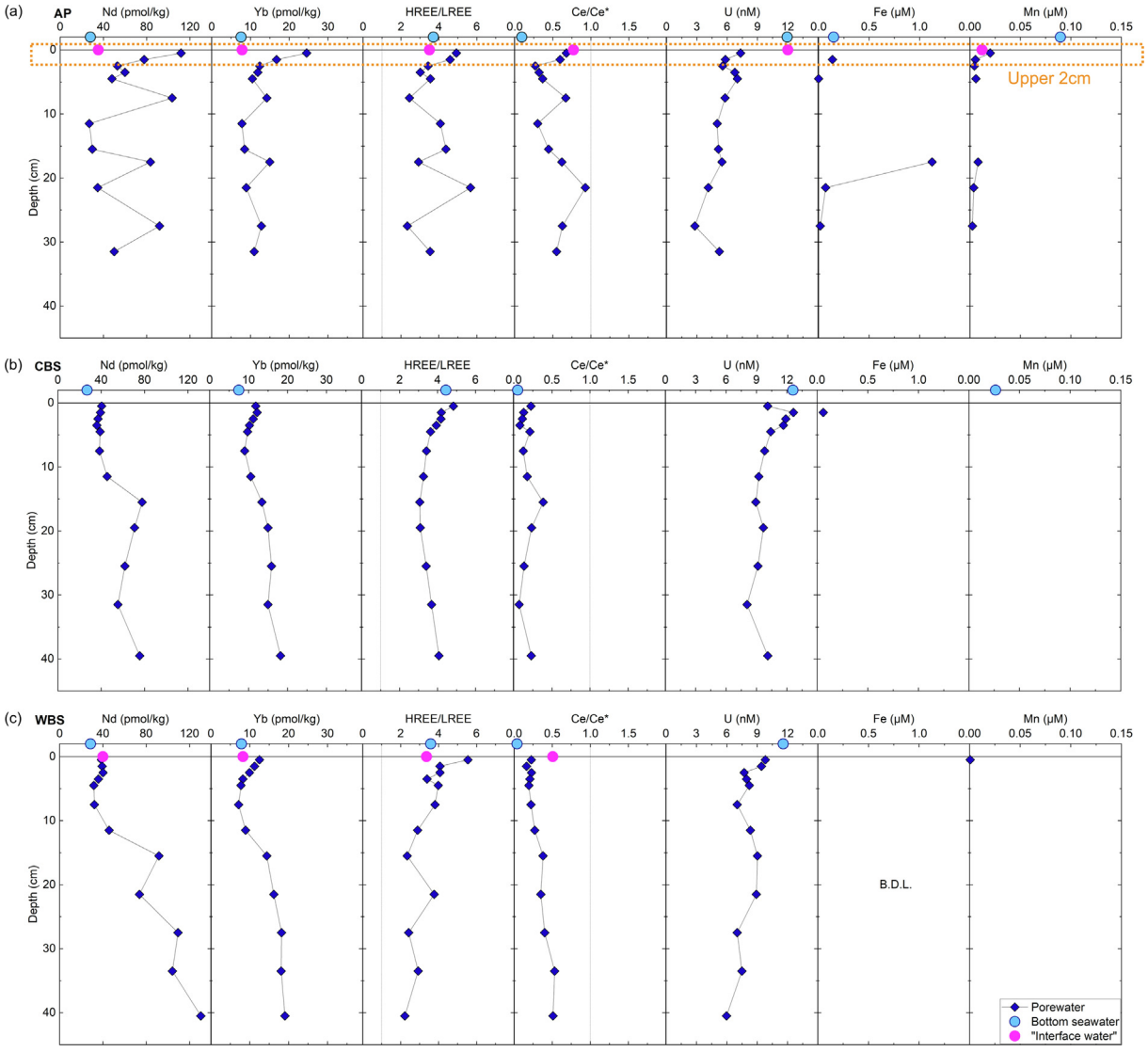

Fig. 3. [Nd], [Yb], HREE/LREE, Ce/Ce*, [U], [Fe], and [Mn] profiles of porewater, bottom water, and "interface water" of study site (a) AP, (b) CBS, and (c) WBS. [Fe] is below the detection limit at WBS for all intervals. Orange rectangle at the AP site highlights the porewater characteristics within the uppermost 2 cm of the seabed.

results from the upward advection of porewaters due to compaction of sediments buried below the redox boundary, and/or downward diffusion from an enriched [U] seawater source to an anoxic sink at depth. Down-core [U] variations might originate from adsorption and/or complexation (Smrzka et al., 2019). Amongst the three study sites, site AP has the lowest [U] and strongest down-core decreasing gradient, probably due to a shallower redox boundary, and therefore lower oxygen content in the porewaters when compared to sites CBS and WBS. This results in more subsurface horizons with detectable dissolved Fe and Mn relative to the other sites. A relatively shallow redox boundary at site AP is also supported by the observation of stronger subsurface maghemite reduction (Channell et al., 2019).

Site AP is located at a significantly shallower water depth than the other two sites (Table 1), and therefore one might expect deeper sub-seafloor bioturbation and, thus, also deeper oxygenation of the seabed at this site (Soetaert et al., 1996; Middelburg et al., 1997). However, due to a shorter sea-ice season both primary productivity (e.g. Del Castillo et al., 2019) and export productivity (Hillenbrand et al., 2003) are significantly higher on the western Antarctic Peninsula margin when compared to the southern Bellingshausen Sea, indicating that oxygen consumption by organic matter degradation is more important than bioturbation for the oxygen content of porewaters in the sub-seafloor sediments.

4.3. Boundary processes in the study area

4.3.1. Benthic Nd flux from porewater to bottom water

The water column at the study sites is characterised by a typical seawater-like REE pattern normalised to PAAS (Post Archean Australian Shale; Taylor and McLennan,

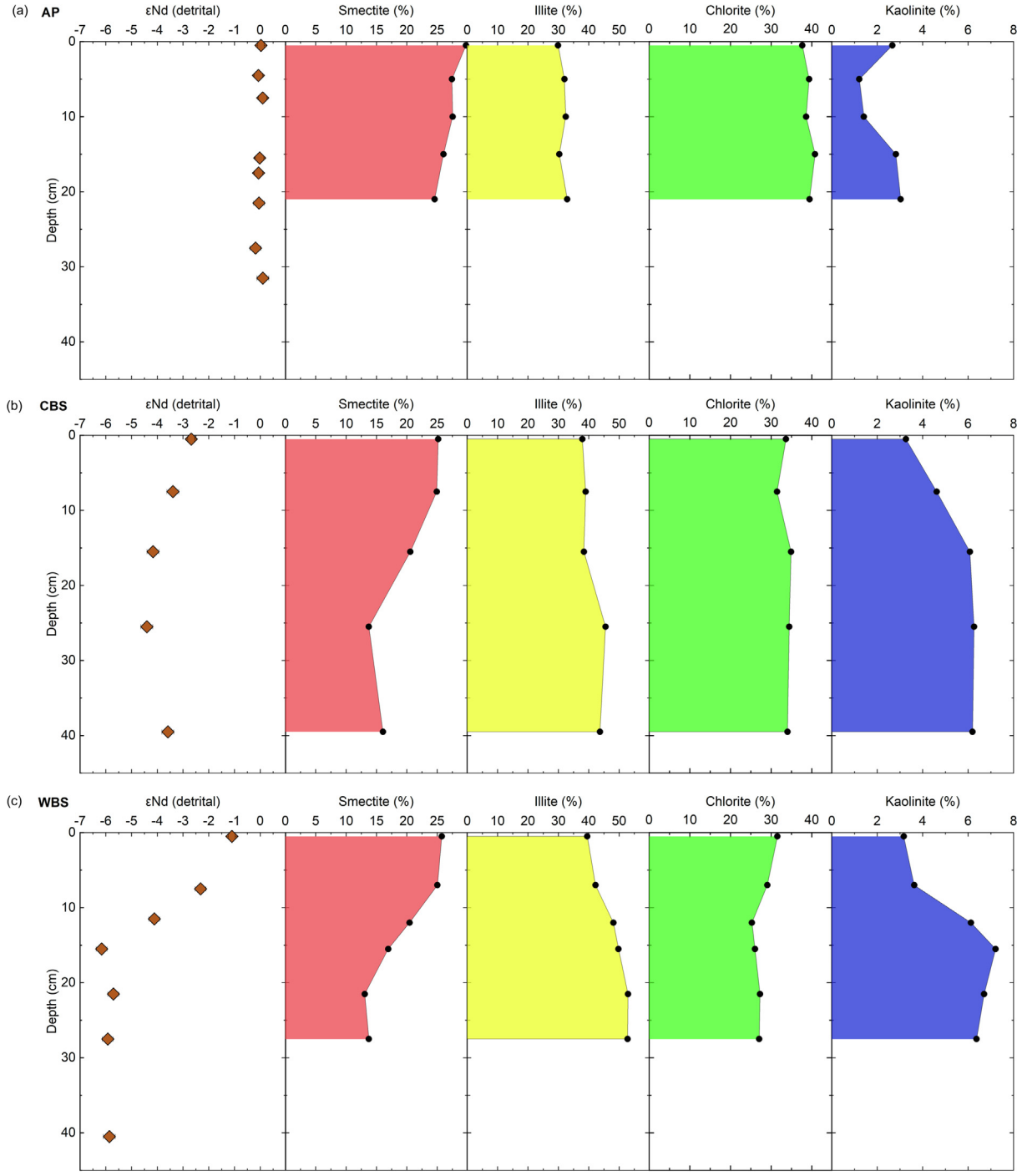

Fig. 4. Down-core εNd composition of detritus < 63 μm and clay mineral composition of the fraction < 2 μm at study sites (a) AP, (b) CBS, and (c) WBS.

1985; Fig. 2 and Fig. 5), with generally increasing $[Nd]_d^{sw}$ and decreasing ratio of HREE/LREE with depth, which results from simple reversible scavenging processes between seawater and particles (Elderfield et al. 1988; Siddall et al., 2008; Wang et al. 2021). The $[Nd]_d^{sw}$ increases at an average rate of about 4 pmol/kg per km water depth at the three studied sites. At site AP, however, $[Nd]_d^{sw}$ shows a major increase of 5 pmol/kg within the lowermost 65 m of the water column, i.e., just above the seafloor. The bottom water $[Nd]_d^{sw}$ at all sites lies in between $[Nd]_d^{sw}$ at shallower water depth and $[Nd]_d^{pw}$ of the uppermost porewater sample. A nepheloid layer above the seabed has been reported from the western Antarctic Peninsula continental margin (Tucholke, 1977) but release of Nd from resuspended particles within this nepheloid layer can be excluded because modification on ε_{Nd} *dsw* has not been observed, despite

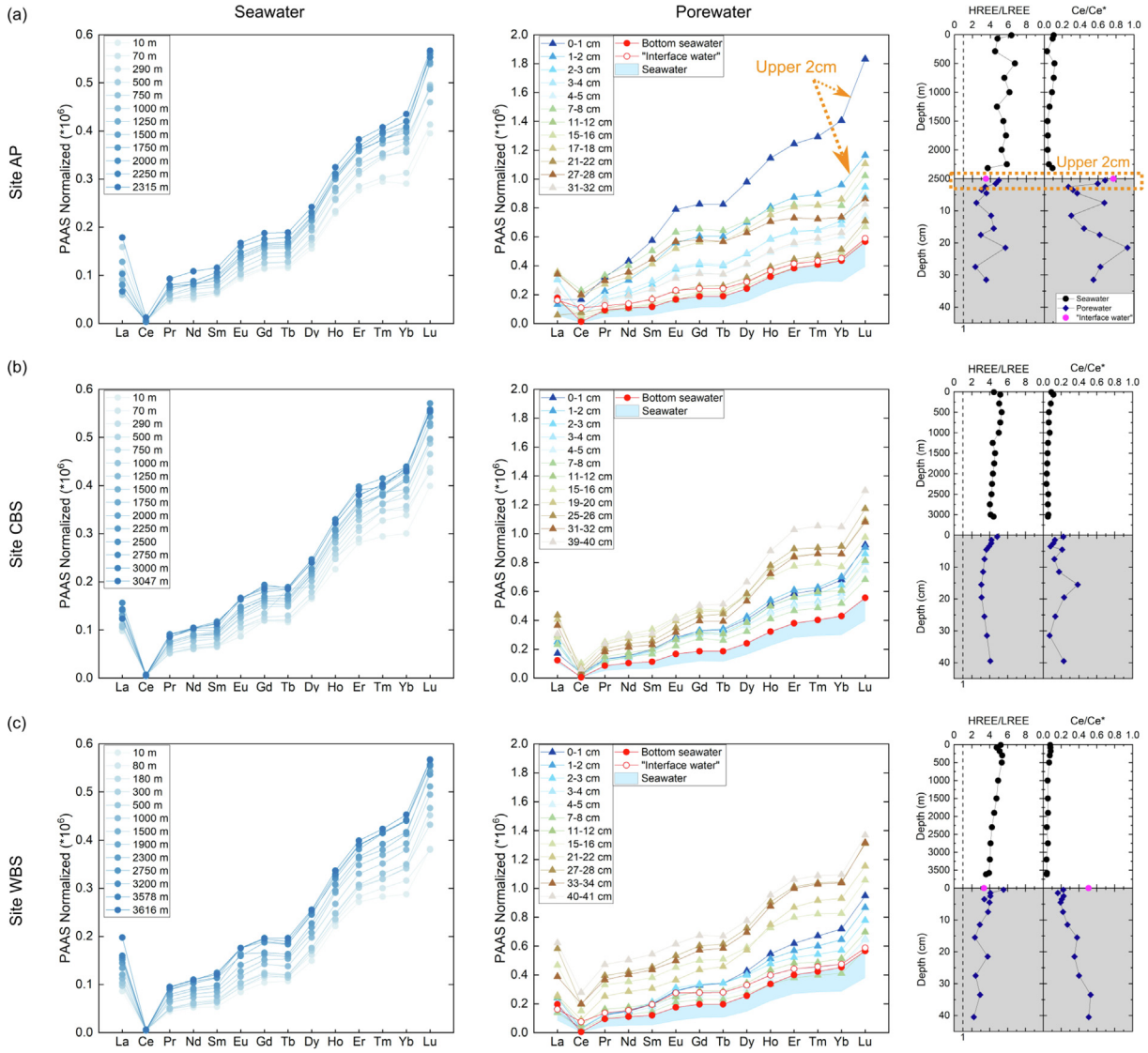

Fig. 5. Dissolved REE normalized to PAAS (Post Archean Australian Shale; Taylor and McLennan, 1985), HREE/LREE, and Ce/Ce* ratios of seawater and porewater of site (a) AP, (b) CBS, and (c) WBS. HREE/LREE = $(Tm_N + Yb_N + Lu_N)/(La_N + Pr_N + Nd_N)$ and the "Ce-anomaly" $Ce/Ce^* = 2*Ce_N/(La_N + Pr_N)$ where subscript $_N$ denotes elements are normalized to PAAS. Orange arrows and rectangle indicate the characteristics of the upper 2 cm porewater of site AP.

the sediment being at least + 5 epsilon unit more radiogenic than the bottom seawater (Fig. 2). Instead, we argue below that the sharp $[Nd]_d^{sw}$ increase observed at the AP site is caused by an upward diffusive flux from sediment porewaters (Hathorne et al., 2015; Crocket et al., 2018).

Dissolved [Nd] within porewaters is higher than in the bottom water at all sites, especially at the AP site, but is still relatively low when compared to global porewater data (Fig. 6). In the upper 10 cm at sites CBS and WBS (Fig. 2b and c), $[Nd]_d^{pw}$ hardly varies down-core and is only marginally higher than in the bottom water. It only increases down-core below ~10 cm sub-bottom depth. The relatively low concentration in the upper 10 cm is possibly the result of bioturbation and lack of sediment consolidation (Hillenbrand et al., 2021) allowing intense exchange between seawater and porewater and between pore spaces. However, at site AP $[Nd]_d^{pw}$ is highest at 0–1 cm depth, i.e., directly below the seawater-sediment interface, and decreases significantly immediately below this depth, before showing very strong down-core variability (Fig. 2a).

We calculate the diffusive REE fluxes from sediment porewaters to the ocean at each core site. Fluxes are estimated from the depth with maximum concentration before the concentration decreases due to other mechanisms. This depth lies at all our study sites at 0–1 cm (Fig. 3), and we use 0.5 cm for calculations. The REE fluxes are calculated following:

$$Flux_{REE} = D_S \frac{\Delta C}{\Delta z} \quad (1)$$

where $\Delta C/\Delta z$ is the concentration gradient between the pore water concentration maximum below the water-

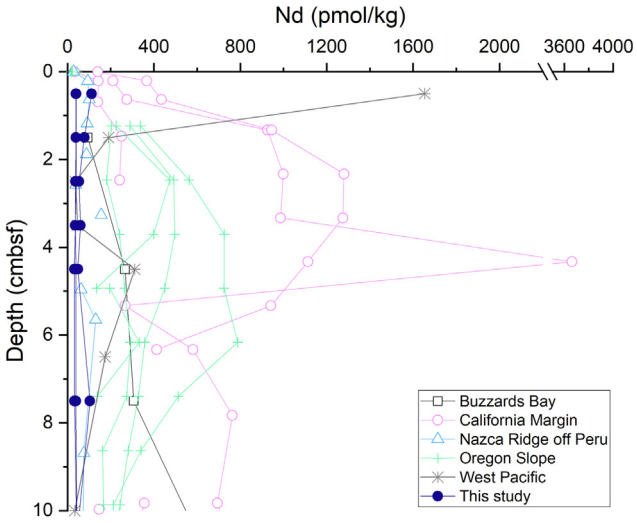

Fig. 6. Global data comparison of dissolved Nd concentrations in porewater within the upper 10 cm of the seabed. Data source: Buzzards Bay, east coast of North America, from Sholkovitz et al. (1989); California margin and Nazca Ridge off Peru from Haley et al. (2004); Oregon slope from Abbott et al. (2015a); West Pacific from Abbott (2019).

sediment interface and the bottom water. D_S is the diffusion coefficient corrected for temperature and tortuosity following Abbott et al. (2015b). D_S was estimated from the relation $D_S = D/(F)$ with the porosity of surface sediments (0.65 as an average of observations; Hillenbrand et al., 2021) and F the formation factor ($F = ^{-n}$ with n = 2.5 for fine grained sediments; Andrews and Bennett, 1981; Ullman and Aller, 1982). Molecular diffusion coefficients (D) for all REEs at 0.4 °C were calculated based on available observations (Li and Gregory, 1974). We used a D of La^{3+} at 0 °C, 18 °C, and 25 °C and Yb^{3+} at 25 °C (Li and Gregory, 1974), while D values for both La^{3+} and Yb^{3+} at 0.4 °C were firstly calculated following the linear relationship between D and temperature displayed by La^{3+}, while assuming that Yb^{3+} has the same relationship. Then D for the other REEs was calculated by a linear extrapolation, leading to lower values of D for HREEs than LREEs (Table S7). Due to the poorly constrained complexation and adsorption of REEs in pore fluids, both processes were not accounted for the estimation of D. All calculated REE fluxes are listed in Table S7. The Nd flux is 7.5 pmol cm^{-2} yr^{-1} at site AP, 1.2 pmol cm^{-2} yr^{-1} at site CBS, and 0.9 pmol cm^{-2} yr^{-1} at site WBS. The relatively high calculated Nd flux at the AP site matches the observed sharp increase of bottom water Nd concentration. We took 0.5 cm as the estimate for Δz which could cause some uncertainty in these calculated benthic fluxes. However, it is important to note that within a global context the Nd flux at the AP site is low, and even negligible at sites CBS and WBS (Fig. 6).

Dissolved Fe and Mn is observable in the bottom water and the subsurface porewater at site AP, which contrasts with the other two sites, where concentrations of dissolved Fe and Mn do not exceed detection limits (Fig. 3). At site AP, Mn is present in detectable quantities close to the subsurface depths as the $[Nd]_d^{pw}$ maxima, and Fe is also present in several depths (Fig. 3). In addition, the Ce anomaly reaches 0.68 within the uppermost 2 cm of the seabed at site AP, and we find that the weakest Ce anomaly (0.77) occurs in the "interface water", while bottom water Ce depletion reaches 0.09 (Fig. 3). The down-core changes of the Ce anomaly co-vary with $[Nd]_d^{pw}$ in the upper 10 cm of the sediment column at site AP ($R^2 = 0.86$); a weaker Ce anomaly, which suggests lower dissolved oxygen content, corresponds to a higher Nd concentration. These observations indicate that the Nd flux is at least partly caused by dissolution of Fe-Mn oxyhydroxides due to changes in the redox environment. In fact, most organic matter deposited on the seabed would be expected to degrade within the upper 1–2 cm of sediment (Hammond et al., 1996), especially in oxic sediment environments which show a markedly faster decomposition rate of organic matter relative to anoxic environments (Haley et al., 2004). The total organic carbon (TOC) content of sediments in the upper 2 cm of the AP site (0.19 wt. %) is lower when compared to the other two sites (0.31 wt. % at site CBS, and 0.24 wt.% at site WBS, respectively; Hillenbrand et al., 2021). Therefore, we suggest that in the upper 2 cm at site AP, the rapid degradation of organic matter on the seabed results in the consumption of oxygen, producing a weaker Ce anomaly and promoting slight dissolution of Fe-Mn oxyhydroxides. Both degradation of organic matter and dissolution of Fe-Mn oxyhydroxides are sources for the Nd input to bottom water at this site. At the other two sites, the Ce anomaly is stronger (<0.51), and less dissolved Fe and Mn (less than half of site AP) are present in the "interface water" and the porewater of the uppermost 2 cm of the sediment column. This indicates that organic matter degradation and Fe-Mn oxyhydroxide dissolution also occur to some extent there. However, we argue that it is not enough to contribute to benthic Nd flux because the oxygen content is higher, which is supported by the very low $[Fe]_d^{pw}$ and $[Mn]_d^{pw}$ as well as high $[U]_d^{pw}$ in comparison with the AP site.

The input of Nd originating from sediment phases into porewater can be inferred from the pronounced increase of the Nd isotopic composition in both the "interface water" and Fe-Mn oxyhydroxide coatings relative to bottom water (Fig. 2). $\varepsilon_{Nd}{}_{d}^{sw}$ ranges from −7 to −9 throughout the water column in the study area (Fig. 2 and Carter et al., 2012). Therefore, the more radiogenic ε_{NdHH} relative to ε_{Nd} *dsw* could not have resulted from the desorption of a seawater Nd isotopic signal from organics or Fe-Mn oxyhydroxides which formed at any level in the water column above the site. Moreover, the ε_{NdHH} gradient towards more radiogenic values with sub-bottom depth, especially within the upper 5–15 cm of the seabed (Fig. 2), suggests a radiogenic isotopic signal which is increasingly released with depth or is diffusing upwards from deeper in the sediment column. Previous research suggested that the ε_{Nd} of porewater may be determined by a highly reactive fraction of the bulk sediment (e.g., Abbott et al., 2015a), and therefore is potentially controlled by changes in sediment chemistry and sedimentation rate. We measured the Nd isotopic composition of detrital sediments < 63 μm, and the results show that at all three sites ε_{Ndsed} is even less radiogenic than ε_{NdHH} below 5–15 cm sediment depth. This indicates that the contribution of Nd from dissolution of detrital particles to porewater within the seabed is not uniform, but strongest from certain particles with a more radiogenic isotopic composition (Wilson et al, 2013; Du et al, 2016).

The REE pattern (Fig. 5) of the porewater has HREE enrichment, which is similar to seawater, rather than a "flat" or "bulged" MREE-enriched pattern, which would be expected from detrital input (e.g. Haley et al., 2004; Abbott et al., 2015b). This likely indicates that dissolved REEs in porewater have been re-scavenged after being released from dissolved detrital particles. This results in a HREE enriched pattern and modification of ε_{Nd} values of porewaters away from the seawater composition, which is later preserved in precipitation of Fe-Mn oxyhydroxide coatings. Moreover, we observe that the lowest porewater REE concentration is observed below 2 cm sub-bottom depth at all three sites, but not at the seawater – sediment interface. We take this as evidence that re-scavenging stops most REE flux from escaping out of the seabed to the ocean, which will be discussed in Sections 4.3.3 and 4.3.4.

4.3.2. Lithological and clay mineralogical sources of Nd

What is the source of the radiogenic Nd which is being added to porewaters? Presence of fine-grained glaciomarine sediments characterises the entire study area (e.g., Rebesco et al. 2002; Pudsey, 2000; Lucchi et al. 2002; Hillenbrand et al., 2003, 2021). Below a thin veneer of sandy to gravelly sediments at the seafloor surface, mud (i.e., clay and silt) is the dominant (80–100 wt.%) grain size in all three analysed box cores (Hillenbrand et al., 2021). Dissolution of detrital particles in the fine-grained fraction is potentially an important source for Nd, and we will first examine their distribution in the study area based on available literature. The composition and geographical distribution of clay mineral assemblages in the fraction < 2 μm of surface sediments on the continental margin of the western Antarctic Peninsula and in the Bellingshausen and Amundsen seas have been extensively investigated (Hillenbrand et al., 2003, 2009; Hillenbrand and Ehrmann, 2005; Ehrmann et al., 2011; Simoes Pereira et al., 2018; Wu et al., 2019). Our study site AP is located offshore from the western Antarctic Peninsula shelf, where sediments are enriched in chlorite and which is therefore referred to as "chlorite province", but influenced by SW-ward bottom current advection of smectite-enriched detritus eroded around the South Shetland Islands, referred to as "smectite province" (Hillenbrand et al., 2003; Hillenbrand and Ehrmann, 2005). Similarly, sites CBS and WBS are located offshore from the southern Bellingshausen Sea shelf, where sediments are enriched in illite and which is consequently referred to as "illite province", but also influenced by bottom-current supply of fine-grained detritus from the chlorite province (Hillenbrand et al., 2003; 2009).

Smectite, which is often formed by subaerial or submarine weathering of volcanic rocks, typically, but not always, has more radiogenic ε_{Nd} values than other clay minerals (Walter, et al. 2000; Bayon et al., 2015; Simoes Pereira et al., 2018; Beny et al., 2020). This is probably reflected at site AP, which is affected by supply of fine-grained detritus derived from the smectite province, and where the highest ε_{Ndsed} values correlate with the highest smectite contents (Fig. 1 and Fig. 4). In contrast to the smectite content, ε_{Ndsed} does not decrease with sub-bottom depth at site AP, but ε_{Ndsed} decreases slightly down-core above ~ 25 cm at site CBS and significantly above ~ 15 cm at site WBS, with corresponding down-core decreases being observed in the smectite contents (Fig. 2 and Fig. 4). This may suggest that at the two Bellingshausen Sea sites input of detritus derived from the volcanic Peter I. Island, where smectite in shelf sediments accounts for up to 81% of the clay mineral assemblage (Hillenbrand et al., 2003), has increased throughout the Holocene. The ε_{Ndsed} is around 0 (Fig. 2) at site AP, which suggests that the ε_{Nd} value of radiogenic detrital particles at this location exceeds 0, given that εNd_{HH} is more radiogenic below ~ 15 cm. A recent study showed that clays supplied by rivers draining an area of volcanic rocks with smectite contents higher than 90% have ε_{Nd} values ranging from −3.2 to 3.8 (Bayon et al., 2015). The ε_{Ndsed} values measured in our study lie within the range of those previously reported from seafloor surface sediments in the region (Roy et al., 2007; Simoes Pereira et al., 2018). The clay mineral data show that the observed down-core decrease of ε_{Ndsed} is accompanied by a decrease of smectite content at sites CBS and WBS, but not site AP (Fig. 4). This indicates that smectite is an important but not the only source controlling ε_{Ndsed}. The XRD records of the clay fraction also document the presence of amphibole (example shown in supplementary Fig. A2), which may also act as a source of Nd.

Tephra that originated from volcanic eruptions in West Antarctica (e.g., Fretzdorff and Smellie, 2002; Dunbar et al., 2008; Hillenbrand et al., 2008b) can also be an important contributor to the radiogenic ε_{Nd} values. Visual observations and volcanic glass particle counts on the coarse sediment fractions > 63 μm and > 500 μm, respectively, have identified the presence of macroscopic tephra and

cryptotephra layers only at sub-bottom depths several meters below our maximum sampling depths (Pudsey, 2000; Lucchi et al., 2002; Hillenbrand et al., 2008b, 2021). Other studies, however, documented the presence of dispersed fine-grained vitric shards in sediment cores from the eastern Pacific sector of the Southern Ocean at shallower sub-bottom depths (Huang et al., 1975; Shane and Froggatt, 1992).

4.3.3. Partial dissolution of detrital particles as a source of Nd in porewaters

We have modelled the effect of partial sediment dissolution and re-scavenging in order to better understand the observed ε_{Nd} and [Nd] of porewaters and authigenic phases at our study sites. We hypothesise that this occurs as a two-stage process. The first stage of the process is likely to be the dissolution of radiogenic detrital particles (smectite, amphibole and/or tephra) which adds Nd to porewaters. The unmodified porewaters are assumed to have an initial Nd concentration and ε_{Nd} composition identical to those of local bottom waters. We use bottom water values averaged from the three study sites as the initial porewater ε_{Nd} and [Nd] values. Based on our clay mineralogical evidence, we use the typical ε_{Nd} values of smectite (Bayon et al., 2015), which ranges from −4 to + 4 for εNd_{add}, as our source of contamination. Conservative mixing curves can be constructed by assuming there is a single source, calculated following.

$$\varepsilon Nd^{pw}_{final} = \frac{[Nd]^{pw}_{initial} * \varepsilon Nd^{pw}_{initial} + ([Nd]^{pw}_{final} - [Nd]^{pw}_{initial}) * \varepsilon Nd_{add}}{[Nd]^{pw}_{final}} \quad (2)$$

where $[Nd]^{pw}_{final}$ and $\varepsilon Nd^{pw}_{final}$ denote the Nd concentration and isotopic composition of porewater after mixing with added Nd, $[Nd]^{pw}_{initial}$ and $\varepsilon Nd^{pw}_{initial}$ represent the values before mixing, and εNd_{add} is the Nd isotopic signal of the detrital source. The resulting mixing curves (Fig. 7), are the plausible envelope of porewater Nd concentration and isotopic composition after process stage 1 (dissolution only).

The second stage of the process is re-scavenging of Nd which lowers the [Nd] but does not change the ε_{Nd} of the porewaters. To represent this, we allow the [Nd] to deviate from a mixing curve between the initial porewater Nd composition (which is identical to that of bottom water) and the detrital Nd source. The degree of re-scavenging varies and produces the scattered deviation from a mixing curve (Fig. 7). Therefore, we need to consider the second stage re-scavenging process to estimate the minimum [Nd] needed for the isotopic modification of the porewater and the potential ε_{Nd} value of the released Nd. We match the data points onto one mixing curve by increasing their concentration to effectively "back-correct" for scavenging (shown as black arrows in Fig. 7 for the different sites).

This model obviously makes a number of assumptions which cannot be constrained, and therefore it does not provide a unique solution to mechanics of the release-re-scavenging process. For example, we only assume a single detrital input source with a constant ε_{Nd} value, dissolution of which increases [Nd] and changes ε_{Nd}. We ascribe deviation from this one mixing curve, as resulting from scavenging, which decreases [Nd] without changing ε_{Nd}. It is possible that additional sources may have been involved, resulting in multiple mixing curves, or multiple stages of release and scavenging may have occurred.

However, despite the simplicity of this model, it is consistent with the large-scale observations in our sedimentological, geochemical, and mineralogical data. For example, for site CBS only one lithological source is necessary as the slight changes shown by detrital Nd isotopes ($\Delta\varepsilon_{Ndsed} < -2$; Fig. 2) is within the estimated ε_{Nd} range of the smectite source (Fig. 7 b). Only a small amount of scavenging is needed, and we observe that more scavenging takes place at greater depth in the sediment, which is consistent with the REE patterns of sediment porewaters.

This modelling also shows that site WBS require two distinct lithogenic sources, with a distinct mixing curve for release above 12 cm sub-bottom depth and a different mixing for samples below 12 cm depth. Examination of the cores from WBS, shows an obvious change in sediment lithology occurring at ~12 cm depth (Hillenbrand et al., 2021). This lithological boundary is also evident in the downcore ε_{Ndsed} and clay mineral data (Fig. 2 and Fig. 4). At site WBS, εNd_{add} lies between −1 and +1 above 15 cm depth and between −4 and −3 below this depth. These εNd_{add} values are largely more radiogenic than those of bulk fine-grained detritus on the adjacent shelves (western Antarctic Peninsula: −3.6 to +2.2, Bellingshausen Sea: −4.3 to −7.2; Simoes Pereira et al., 2018), supporting our hypothesis of preferential dissolution of radiogenic particles, such as smectite, amphibole and/or volcanic glass.

It is plausible to explain the observed trends in [Nd] and ε_{Nd} as a result of diffusion from a single source sediment horizon (such as a distinct tephra layer) that sits below the base of our cores and diffuses upwards through the sediment column. However, the WBS site places an important constraint on this process because it is most simple ascribed by assuming two different sources and therefore two mixing curve (Fig. 7c). The boundary between these two sources occurs at 12 cm sub-bottom depth, which is marked by a clear change in sediment provenance and a lithological boundary (Fig. 2 and Fig. 4; Hillenbrand et al., 2021). Despite the porewaters diffusing upwards, this offset in their porewater chemistry occurs at the same depth as the lithological boundary, which implies that dissolved Nd is being continuously released at all depths. This indicates a relatively low dissolution and diffusion rate versus sedimentation rate.

We can estimate the amount of $[Nd]_{add}$ that is required to cause the ε_{Nd} changes in porewater in different layers according to the model. We chose 6 ppt (42 pmol/kg) and 20 ppt (139 pmol/kg) as $[Nd]^{pw}_{final}$ at the shallowest and deepest depths in core CBS as an example, thus about 2 ppt (14 pmol/kg) and 16 ppt (111 pmol/kg) of Nd is needed ($[Nd]_{add} = [Nd]^{pw}_{final} - [Nd]^{pw}_{initial}$), respectively. With the measured mass ratio of porewater/sediment (which ranges from 4 to 0.57 with depth), Nd concentration of a radiogenic particle, e.g. smectite (average value 19.3 ppm, Bayon et al., 2015), and smectite content in bulk sediment (25–15% smectite in clay minerals with depth shown in Fig. 4

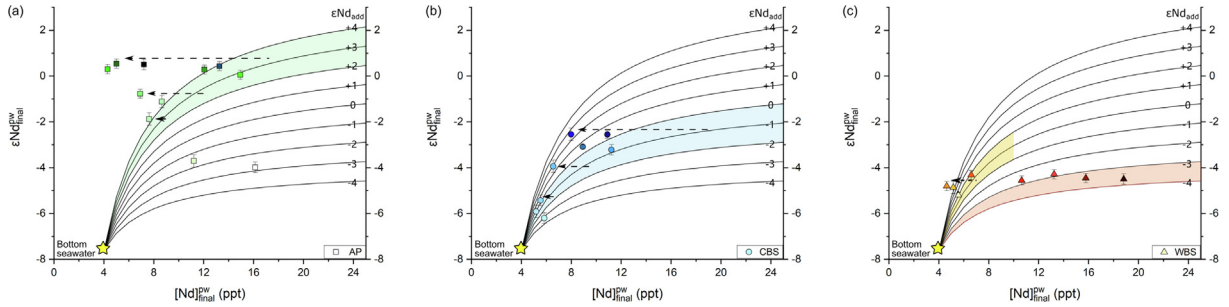

Fig. 7. Mixing curves between initial porewater Nd concentration and εNd value (=bottom water) and release of Nd by dissolution of radiogenic detrital particles with different ε_{Nd} values, with (a) all porewater data; and the estimation of the minimum Nd flux required to cause the ε_{Nd} change in porewater and the most likely ε_{Nd} value of the dissolved detritus for site (b) AP, (c) CBS, and (d) WBS. ε_{Nd} values of dissolved detrital particles chosen for mixing curves range from −4 to + 4 (=ε_{Nd} values for different smectite minerals taken from Bayon et al., 2015). Squares, dots, and triangles denote porewater data at sites AP, CBS, and WBS, respectively, with lighter to darker colours indicating shallower to deeper sub-bottom depths. Grey symbols and black arrows show the matching of data points to a particular mixing curve allowing for variable Nd removal by scavenging. Coloured shaded areas between mixing curves indicate the most likely range of the $\varepsilon_{Nd\ add}$ value of the dissolved detritus.

and ~ 80% clay minerals in the clay fraction (<2 micron), which constitutes 20–80% of bulk sediments (on average 50%) in this area (Hillenbrand et al. (2021)), we can estimate the amount of particle dissolution. The estimation indicates that about 1–3 ppm of smectite dissolution is required. The uncertainty of the estimation is within a few ppm and assumes a smectite source of the radiogenic signal. The dissolution could be different for other radiogenic particles. Also, we cannot exclude minor Nd contributions from dissolution of other, less radiogenic detrital particles. The variability of the estimated εNd_{add} could be the result of different chemical compositions and relative solubility of smectite, amphibole and/or volcanic glass deposited at the different sites (c.f., Park et al., 2019). It can also be contributed by partial dissolution of other particles in the fine-grained fraction, e.g. of the clay minerals chlorite, illite, or kaolinite, which would imply less radiogenic εNd_{add}. The latter is a more likely scenario for site WBS in particular, because it requires two mixing curves in order to fit the data.

4.3.4. Potential formation of secondary minerals as a sink of REE in porewater

If there was only addition of Nd to the porewater within the sediment column caused by dissolution of radiogenic particles and other clay minerals, the shape of porewater REE pattern would be modified to the "flat" or "bulged" shape of these particles (e.g. Abbott et al., 2015b; Bayon et al., 2015). We did not observe porewater REE pattern similar to detrital particles (Fig. 5). Therefore, formation of secondary minerals and re-scavenging must occur to re-store the HREE enrichment pattern of the porewater. A wide range of secondary minerals, including Fe-Mn oxyhydroxides, phyllosilicates, and phosphates that preferentially scavenge LREEs, resulting in HREE enrichment in porewater are known to form during early diagenesis (Cantrell and Byrne, 1987; Byrne and Kim, 1990; Koeppenkastrop and De Carlo, 1993; Bayon et al., 2004). We propose the formation of Fe-Mn oxyhydroxides dominates the re-scavenging, the presence of which is shown by the very low dissolved Fe and Mn concentrations in the porewater (sub-nM, Fig. 3). Moreover, the ε_{Nd} signal from leachates, which records the porewater modification caused by dissolution of radiogenic particles at different sub-bottom depths, suggests that the Fe-Mn oxyhydroxides form after detrital input. We rule out the influence of clay mineral formation, such as glauconite suggested by Abbott et al. (2019), because new formation of such clay minerals has not been observed in previous studies of Quaternary sediments from this region (Hillenbrand et al., 2003, 2009, 2021; Hillenbrand and Ehrmann, 2005; Wu et al., 2019).

At all study sites the HREE/LREE ratio in the porewater reaches its maximum above 2 cm sub-bottom depth, while the Nd isotope modification is at its minimum (Fig. 2 and Fig. 5). This cannot be explained by simple partial dissolution of radiogenic fine-grained particles followed by re-scavenging because a maximum HREE/LREE ratio and an increased Nd concentration would result from a relatively high input and removal rate, which would shift the ε_{Nd} of porewater to more radiogenic values. In fact, within the surface sediment layer active biological processes occur, which include the decomposition of organic matter and minor dissolution of Fe-Mn oxyhydroxides, which contributes a REE flux (as discussed in Section 4.3.1). Organic matter preferentially adsorbs LREEs, whereas HREEs form more stable dissolved carbonate complexes in solution (Cantrell and Byrne, 1987; Byrne and Kim, 1990). Therefore, organic matter degradation usually results in flatter REE patterns in solution. However, partial remineralization of particulate organic carbon (POC) can contribute to HREE enrichment in porewaters due to preferential release of HREEs over LREEs (Haley et al., 2004; Kim et al., 2012), which may explain our observation.

4.4. Boundary processes on the West Antarctic continental margin

The data in this study can be explained by a sequence of boundary processes (Fig. 8) which are summarised as: (1)

porewater with an initial [REE] and ε_{Nd} signature of seawater; (2) partial remineralization of organic matter and minor dissolution of Fe-Mn oxyhydroxides in the upper 2 cm; (3) partial dissolution of detrital radiogenic particles (smectite, amphibole, tephra and potentially other clay minerals) through all sub-bottom depths, simultaneously increasing [REE], changing REE patterns and modifying ε_{Nd} of porewater; (4) re-scavenging by Fe-Mn oxyhydroxide (and probably other secondary minerals), which lowers [REE] and thus re-establishes a seawater-like REE pattern and records the ε_{Nd} value of porewater; (5) Nd flux from porewater to bottom water, causing [REE] of bottom water slightly to increase with no significant ε_{Nd} modification.

On the continental rise west of the Antarctic Peninsula and in the Bellingshausen Sea, we observe two boundary processes. There is a modification of porewater ε_{Nd} to a more radiogenic value due to partial dissolution of radiogenic fine-grained detritus in seabed sediments (primarily smectite, amphibole and/or volcanic glass), followed by re-scavenging onto Fe-Mn oxyhydroxides. This process shifts the ε_{Nd} signature of porewaters from that of local bottom water to more radiogenic values without increasing the Nd concentration. This process appears to be similar to what has been termed "boundary exchange" processes observed in the water column, but in our study area it occurs only in the sediment porewaters. This is followed by benthic flux which is enhanced by partial decomposition of organic matter and minor dissolution of Fe-Mn oxyhydroxides in the upper 2 cm of the seabed sediments, and is best observed at site AP resulting in an increase Nd concentration of bottom water.

The benthic Nd flux from porewater to seawater in the study area (maximum 7.5, 1.2, and 0.9 pmol cm-^{2} yr^{-1} at site AP, CBS, and WBS, respectively) is an order of magnitude lower in comparison with other measurements of benthic fluxes, for example on the California margin (~40 pmol cm^{-2} yr^{-1} at 3400 m water depth, Haley et al., 2004), Oregon slope (32 pmol cm^{-2} yr^{-1} at 3000 m water depth, Abbott et al., 2015b), and in the Tasman Sea (25.1 pmol cm^{-2} yr^{-1} at 1500 m water depth, Abbott, 2019). This is a result of both reduced contribution from dissolution of radiogenic particles and enhanced re-scavenging. Moreover, on the California margin and Oregon slope, porewaters contain up to 80 μM dissolved Fe and 60 μM dissolved Mn, indicating significant contributions from dissolution of Fe-Mn oxyhydroxides. In contrast, Fe and Mn are primarily present in form of oxyhydroxides in the sediments of our study sites, and these Fe-Mn oxyhydroxides re-scavenge REEs released by dissolution of fine-grained radiogenic detritus, which further reduces dissolved [Nd] in porewater. Compared to studies from other sites globally, the calculated benthic flux, even

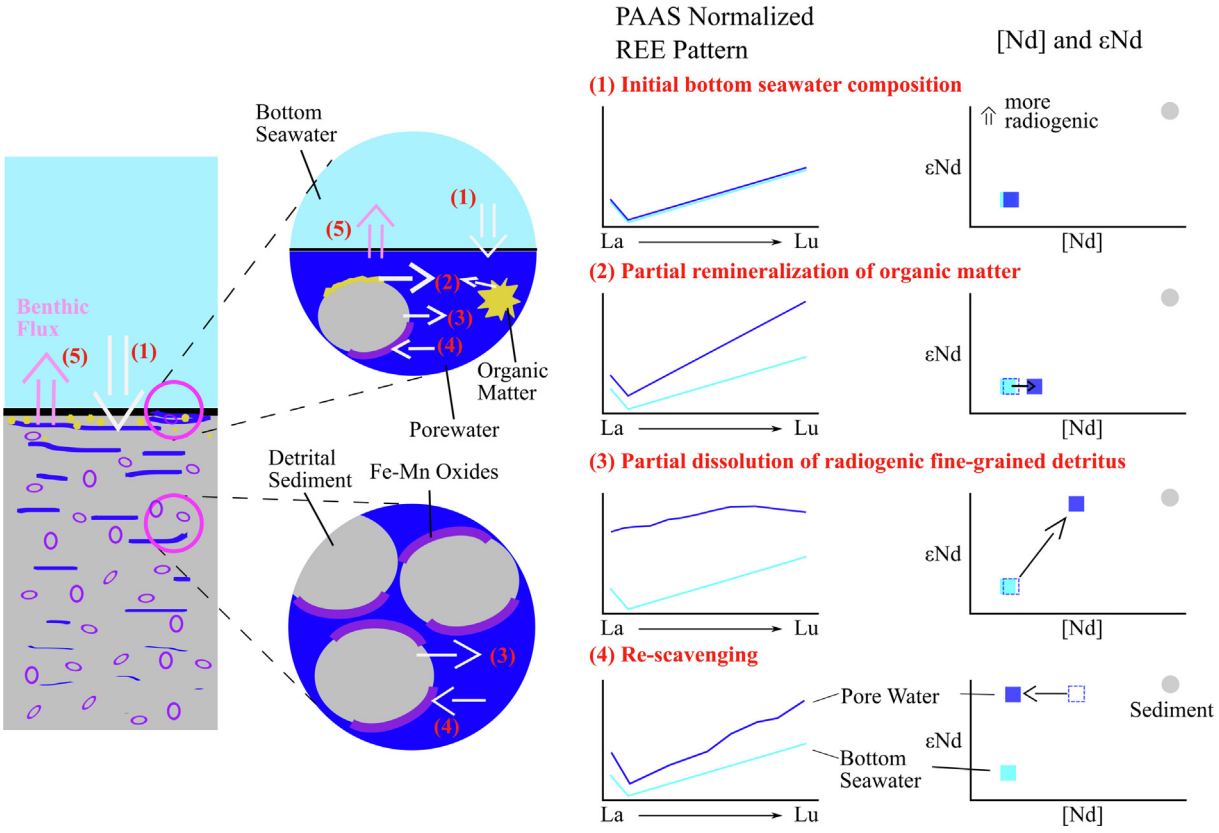

Fig. 8. Schematic description of boundary processes on the West Antarctic continental margin. The four steps of boundary processes are illustrated in the cartoons on the left; and the corresponding changes of REE patterns, [Nd] and ε_{Nd} with every step are shown in the right panels.

at site AP, is relatively minor. This suggests that there is little Nd input from West Antarctic continental margin sediments to the ocean.

However, numerous fluid-escape structures documenting the escape of interstitial fluids originating from deep within the seabed at the seafloor surface have been observed on the Pacific margin of the Antarctic Peninsula, both in reflection seismic profiles (e.g., Volpi et al., 2003) and acoustic sub-bottom profiler data (Fig. S4 in Hillenbrand et al., 2021). The associated benthic flux of porewater through these fluid-escape structures apparently originates from the diagenetic transition of opal A to opal CT at depth in the sediment column (Volpi et al., 2003) but the extent of this input and its implication for Nd and REE needs to be further constrained in future studies.

In several previously published seawater profiles on the West Antarctic continental rise the ε_{Nd} values become more radiogenic near the seabed, with minor accompanying increases in [Nd] recorded in two profiles from the western Antarctic Peninsula and Bellingshausen Sea rise, respectively (Carter et al., 2012), and a clear [Nd] increase only observed in a profile from one of the volcanic Marie Byrd Seamounts in the Amundsen Sea (Rickli et al., 2014). This suggests that boundary exchange is the major benthic process on the continental rise in the Bellingshausen Sea and possibly Amundsen Sea, while benthic flux is likely more important on the western Antarctic Peninsula continental rise as shown in this study. On the West Antarctic continental shelf, benthic flux prevails and supplies Nd to bottom water due to dissolution of radiogenic detrital particles (Carter et al., 2012). We cannot exactly identify the source of a more radiogenic ε_{Nd} signal from sediment dissolution on the West Antarctic continental margin but we hypothesize that it is predominantly smectite, amphibole, volcanic glass or a combination of these particles, which are widespread in the fine-grained fraction of these sediments (Fig. 4, Fig. A4; Huang et al., 1975; Shane and Froggatt, 1992; Hillenbrand et al., 2003, 2009, 2021; Hillenbrand and Ehrmann, 2005; Ehrmann et al., 2011; Simoes Pereira et al., 2018; Wu et al., 2019).

Roy et al. (2007) measured Nd isotopes in detrital core-top sediments (<63 μm fraction) mainly at deep-water sites on the circum-Antarctic margin to track sediment sources on the continent. The results showed that more radiogenic ε_{Nd} values and associated young Sm/Nd-model ages characterize sediments near West Antarctica, while less radiogenic ε_{Nd} value and older Sm/Nd-model ages are found in samples proximal to East Antarctica, consistent with the geology of these parts of the Antarctic continent (cf. Walter et al., 2000; Pierce et al., 2011; Cook et al., 2013; Simoes Pereira et al., 2018; Robinson et al., 2021; Huang et al., 2021). Accordingly, the boundary processes on the East Antarctic continental margin, if they take place, will tend to shift the Nd isotopic ratios of bottom water to less radiogenic values. Seawater Nd data from the Weddell Gyre show that boundary exchange processes occur on the continental margin of western Dronning Maud Land that shift ε_{Nd} of AABW in the Atlantic sector to less radiogenic values (average $\varepsilon_{Nd} = -9$) relative to LCDW (Stichel et al., 2012). In the southern Weddell Sea, however, no obvious modification of [Nd] or ε_{Nd} was observed on the continental shelf in front of the Filchner-Rønne Ice Shelf (Huang et al., 2021). Better constraining the boundary processes on the East and West Antarctic continental margins requires further research, incorporating coordinated collection of seawater, porewater, and sediment samples from different sectors and water depths.

Leachates of Fe-Mn oxyhydroxide coatings in marine sediment cores are widely utilized to extract ε_{Nd} signals in order to reconstruct palaeo bottom water circulation in areas, where no obvious boundary processes exist (e.g. Piotrowski et al., 2004; Piotrowski et al., 2005; Howe et al., 2016). On the West Antarctic continental margin, however, ε_{Nd} values of Fe-Mn oxyhydroxide coatings do not represent a bottom water signal due to Nd release from dissolved fine-grained detritus into porewater. The extent of ε_{Nd} modification is likely determined by the proportion of the reactive detrital particles, as observed in this study and previous studies (Blaser et al., 2016; Du et al., 2016). Consequently, palaeoceanographic studies based on the ε_{Nd} signal extracted from Fe-Mn oxyhydroxide in West Antarctic continental margin sediments will most likely be unreliable. On the East Antarctic margin, a case study conducted in the Weddell Sea has shown that ε_{Nd} of leachates can match the bottom water value (Huang et al., 2021). However, as the ε_{Nd} signature of seawater can be driven by a small reactive fraction of the bulk sediment, it is probably sensitive to even small shifts in sediment provenance (Wilson et al., 2012). Therefore, detailed studies on various parts of the Antarctic continental margin are required to test the reliability of the ε_{Nd} signal extracted by leaching of Fe-Mn oxyhydroxide in marine sediments as a palaeoceanographic proxy.

5. CONCLUSIONS

Boundary processes are observed on the Pacific margin of West Antarctica, but do not greatly change the Nd isotopic composition of bottom waters. The dominant boundary exchange process occurs in porewaters and results from the incongruent dissolution of radiogenic fine-grained detritus (probably smectite, amphibole and/or tephra) and later re-scavenging due to formation of secondary minerals, especially Fe-Mn oxyhydroxides. This alters the Nd isotopic composition of porewaters without greatly increasing Nd concentration. This is followed by benthic flux of these porewaters into bottom waters, and is enhanced by the partial decomposition of organic matter and potentially partial dissolution of Fe-Mn oxyhydroxides, mainly at the seabed surface (i.e. the upper 2 cm). By comparing the geochemistry of porewaters, authigenic oxides, and sediment, as well as sediment lithology and mineralogy, we were able to link these processes to their chemical and lithological control. The boundary processes on the West Antarctic continental rise change porewater chemistry to more radiogenic values, but due to the low Nd concentrations and Nd flux from porewaters to bottom waters, they do not appear to modify the Nd isotopic composition of bottom water. The diage-

netic modification of porewaters and Fe-Mn oxyhydroxides in marine sediments from the West Antarctic margin complicate palaeoceanographic studies in this area.

Declaration of Competing Interest

The authors declare that they have no known competing financial interests or personal relationships that could have appeared to influence the work reported in this paper.

ACKNOWLEDGEMENT

We thank the captain, officers, crew, technical support staff and shipboard scientists of RRS *James Clark Ross* cruise JR298. We especially thank Robert Larter (BAS) for planning and leading the cruise. Furthermore, we are grateful to J. Clegg and M. Greaves (University of Cambridge) for assistance with laboratory analyses, and A. Turchyn (University of Cambridge) for providing sample processing equipment.

This study forms part of the British Antarctic Survey's *Polar Science for Planet Earth* Programme and was made possible by NERC UK-IODP grants NE/J006513/1 and NE/J006548/1, a NERC funded PhD project to T. Williams, and a NERC collaborative gearing scheme grant to support A. Piotrowski and T. Williams for participating in cruise JR298. Ruixue Wang is supported by CSC Cambridge International Scholarship jointly funded by Cambridge TRUST and China Scholarship Council.

APPENDIX A. SUPPLEMENTARY MATERIAL

Supplementary data to this article can be found online at https://doi.org/10.1016/j.gca.2022.04.012.

REFERENCES

Abbott A. N. (2019) A benthic flux from calcareous sediments results in non-conservative neodymium behavior during lateral transport: A study from the Tasman Sea. *Geology* **47**, 363–366.

Abbott A. N., Haley B. A. and McManus J. (2015a) Bottoms up: Sedimentary control of the deep North Pacific Ocean's εNd signature. *Geology* **43**, 1035–1038.

Abbott A. N., Haley B. A., McManus J. and Reimers C. E. (2015b) The sedimentary flux of dissolved rare earth elements to the ocean. *Geochim. Cosmochim. Acta* **154**, 186–200.

Abbott A. N., Löhr S. and Trethewy M. (2019) Are clay minerals the primary control on the oceanic rare earth element budget? *Front. Mar. Sci.* **6**, 1–19.

Andrews D. and Bennett A. (1981) Measurements of diffusivity near the sediment-water interface with a fine-scale resistivity probe. *Geochim. Cosmochim. Acta* **45**, 2169–2175.

Arsouze T., Dutay J. C., Lacan F. and Jeandel C. (2009) Reconstructing the Nd oceanic cycle using a coupled dynamical–biogeochemical model. *Biogeosciences* **6**(12), 2829–2846.

Basak C., Pahnke K., Frank M., Lamy F. and Gersonde R. (2015) Neodymium isotopic characterization of Ross Sea Bottom Water and its advection through the southern South Pacific. *Earth Planet. Sci. Lett.* **419**, 211–221.

Bau M., Koschinsky A., Dulski P. and Hein J. R. (1996) Comparison of the partitioning behaviours of yttrium, rare earth elements, and titanium between hydrogenetic marine ferromanganese crusts and seawater. *Geochim. Cosmochim. Acta* **60**, 1709–1725.

Bayon G., German C. R., Burton K. W., Nesbitt R. W. and Rogers N. (2004) Sedimentary Fe-Mn oxyhydroxides as paleoceanographic archives and the role of aeolian flux in regulating oceanic dissolved REE. *Earth Planet. Sci. Lett.* **224**, 477–492.

Bayon G., Toucanne S., Skonieczny C., André L., Bermell S., Cheron S., Dennielou B., Etoubleau J., Freslon N., Gauchery T., Germain Y., Jorry S. J., Ménot G., Monin L., Ponzevera E., Rouget M. L., Tachikawa K. and Barrat J. A. (2015) Rare earth elements and neodymium isotopes in world river sediments revisited. *Geochim. Cosmochim. Acta* **170**, 17–38.

Beny F., Bout-Roumazeilles V., Davies G. R., Waelbroeck C., Bory A., Tribovillard N., Delattre M. and Abraham R. (2020) Radiogenic isotopic and clay mineralogical signatures of terrigenous particles as water-mass tracers: New insights into South Atlantic deep circulation during the last termination. *Quat. Sci. Rev.* **228**, 106089.

Blaser P., Lippold J., Gutjahr M., Frank N., Link J. M. and Frank M. (2016) Extracting foraminiferal seawater Nd isotope signatures from bulk deep sea sediment by chemical leaching. *Chem. Geol.* **439**, 189–204.

Byrne R. H. and Kim K. H. (1990) Rare earth element scavenging in seawater. *Geochim. Cosmochim. Acta* **54**, 2645–2656.

Camerlenghi A., Crise A., Pudsey C. J., Accerbonm E., Laterza R. and Rebesco M. (1997) Ten-month observation of the bottom current regime across a sediment drift of the Pacific margin of the Antarctic Peninsula. *Antarct. Sci.* **9**, 426–433.

Cantrell K. J. and Byrne R. H. (1987) Rare earth element complexation by carbonate and oxalate ions. *Geochim. Cosmochim. Acta* **51**, 597–605.

Carter P., Vance D., Hillenbrand C. D., Smith J. A. and Shoosmith D. R. (2012) The neodymium isotopic composition of waters masses in the eastern Pacific sector of the Southern Ocean. *Geochim. Cosmochim. Acta* **79**, 41–59.

Del Castillo C. E., Signorini S. R., Karaköylü E. M. and Rivero-Calle S. (2019) Is the Southern Ocean getting greener? *Geophys. Res. Lett.* **46**, 6034–6040.

Channell J. E. T., Xuan C., Hodell D. A., Crowhurst S. J. and Larter R. D. (2019) Relative paleointensity (RPI) and age control in Quaternary sediment drifts off the Antarctic Peninsula. *Quat. Sci. Rev.* **211**, 17–33.

Cook C. P., Van De Flierdt T., Williams T., Hemming S. R., Iwai M., Kobayashi M., Jimenez-Espejo F. J., Escutia C., González J. J., Khim B. K., McKay R. M., Passchier S., Bohaty S. M., Riesselman C. R., Tauxe L., Sugisaki S., Galindo A. L., Patterson M. O., Sangiorgi F., Pierce E. L., Brinkhuis H., Klaus A., Fehr A., Bendle J. A. P., Bijl P. K., Carr S. A., Dunbar R. B., Flores J. A., Hayden T. G., Katsuki K., Kong G. S., Nakai M., Olney M. P., Pekar S. F., Pross J., Röhl U., Sakai T., Shrivastava P. K., Stickley C. E., Tuo S., Welsh K. and Yamane M. (2013) Dynamic behaviour of the East Antarctic ice sheet during Pliocene warmth. *Nat. Geosci.* **6**, 765–769.

Crocket K. C., Hill E., Abell R. E., Johnson C., Gary S. F., Brand T. and Hathorne E. C. (2018) Rare earth element distribution in the ne Atlantic: Evidence for benthic sources, longevity of the seawater signal, and biogeochemical cycling. *Front. Mar. Sci.* **5**, 1–22.

Cunningham A. P., Larter R. D., Barker P. F., Gohl K. and Nitsche F. O. (2002) Tectonic evolution of the Pacific margin of Antarctica 2. Structure of Late Cretaceous-early Tertiary plate boundaries in the Bellingshausen Sea from seismic reflection and gravity data. *J. Geophys. Res. Solid Earth* **107**, EPM-6.

Dausmann V. (2018) Present and past changes in continental weathering and ocean circulation from radiogenic Nd, Hf and Pb isotopes. (Doctoral dissertation).

Dowdeswell J. A., Cofaigh C. Ó., Noormets R., Larter R. D., Hillenbrand C. D., Benetti S., Evans J. and Pudsey C. J. (2008) A major trough-mouth fan on the continental margin of the Bellingshausen Sea, West Antarctica: The Belgica Fan. *Mar. Geol.* **252**, 129–140.

Du J., Haley B. A. and Mix A. C. (2016) Neodymium isotopes in authigenic phases, bottom waters and detrital sediments in the Gulf of Alaska and their implications for paleo-circulation reconstruction. *Geochim. Cosmochim. Acta* **193**, 14–35.

Duce R. A., Liss P. S., Merrill J. T., Atlas E. L., Buat-Menard P., Hicks B. B., Miller J. M., Prospero J. M., Arimoto R., Church T. M., Ellis W., Galloway J. N., Hansen L., Jickells T. D., Knap A. H., Reinhardt K. H., Schneider B., Soudine A., Tokos J. J., Tsunogai S., Wollast R. and Zhou M. (1991) The atmospheric input of trace species to the world ocean. *Global Biogeochem. Cycles* **5**, 193–259.

Dunbar N. W., McIntosh W. C. and Esser R. P. (2008) Physical setting and tephrochronology of the summit caldera ice record at Mount Moulton, West Antarctica. *Bull. Geol. Soc. Am.* **120**, 796–812.

Ehrmann W., Hillenbrand C. D., Smith J. A., Graham A. G. C., Kuhn G. and Larter R. D. (2011) Provenance changes between recent and glacial-time sediments in the Amundsen Sea embayment, West Antarctica: Clay mineral assemblage evidence. *Antarct. Sci.* **23**, 471–486.

Ehrmann W. U., Melles M., Kuhn G. and Grobe H. (1992) Significance of clay mineral assemblages in the Antarctic Ocean. *Mar. Geol.* **107**, 249–273.

Elderfield H., Whitfield M., Burton J. D., Bacon M. P. and Liss P. S. (1988) The oceanic chemistry of the rare-earth elements. *Philos. Trans. Roy. Soc. A Math. Phys. Eng. Sci.* **325**, 105–126.

Frank M. (2002) Radiogenic isotopes: Tracers of past ocean circulation and erosional input. *Rev. Geophys.* **40**, 1.

Fretzdorff S. and Smellie J. L. (2002) Electron microprobe characterization of ash layers in sediments from the central Bransfield basin (Antarctic Peninsula): Evidence for at least two volcanic sources. *Antarct. Sci.* **14**, 412–421.

Giorgetti A., Crise A., Laterza R., Perini L., Rebesco M. and Camerlenghi A. (2003) Water masses and bottom boundary layer dynamics above a sediment drift of the Antarctic Peninsula Pacific Margin. *Antarct. Sci.* **15**, 537–546.

Goldstein S. J. and Jacobsen S. B. (1987) The Nd and Sr isotopic systematics of river-water dissolved material: Implications for the sources of Nd and Sr in seawater. *Chem. Geol. Isot. Geosci. Sect.* **66**, 245–272.

Goldstein S. L. and Hemming S. R. (2003) Long-lived isotopic tracers in oceanography, paleoceanography, and ice-sheet dynamics. *Treatise Geochem.* **6**, 625.

Goldstein S. L., O'Nions R. K. and Hamilton P. J. (1984) A SmNd isotopic study of atmospheric dusts and particulates from major river systems. *Earth Planet. Sci. Lett.* **70**, 221–236.

Greaves M. J., Elderfield H. and Klinkhammer G. P. (1989) Determination of the rare earth elements in natural waters by isotope-dilution mass spectrometry. *Anal. Chim. Acta* **218**, 265–280.

Grousset F. E., Biscaye P. E., Zindler A., Prospero J. and Chester R. (1988) Neodymium isotopes as tracers in marine sediments and aerosols: North Atlantic. *Earth Planet. Sci. Lett.* **87**, 367–378.

Grousset F. E., Parra M., Bory A., Martinez P., Bertrand P., Shimmield G. and Ellam R. M. (1998) Saharan wind regimes traced by the Sr-Nd isotopic composition of subtropical Atlantic sediments: Last Glacial Maximum vs today. *Quat. Sci. Rev.* **17**, 395–409.

Haley B. A., Klinkhammer G. P. and McManus J. (2004) Rare earth elements in pore waters of marine sediments. *Geochim. Cosmochim. Acta* **68**, 1265–1279.

Hammond D. E., McManus J., Berelson W. M., Kilgore T. E. and Pope R. H. (1996) Early diagenesis of organic material in equatorial Pacific sediments: stpichiometry and kinetics. *Deep Sea Res. Part II Top. Stud. Oceanogr.* **43**, 1365–1412.

Hathorne E. C., Stichel T., Brück B. and Frank M. (2015) Rare earth element distribution in the Atlantic sector of the Southern Ocean: The balance between particle scavenging and vertical supply. *Mar. Chem.* **177**, 157–171.

Hernández-Molina F. J., Larter R. D. and Maldonado A. (2017) Neogene to Quaternary stratigraphic evolution of the Antarctic Peninsula, Pacific Margin offshore of Adelaide Island: Transitions from a non-glacial, through glacially-influenced to a fully glacial state. *Glob. Planet. Change* **156**, 80–111.

Hillenbrand C. D., Baesler A. and Grobe H. (2005) The sedimentary record of the last glaciation in the western Bellingshausen Sea (West Antarctica): Implications for the interpretation of diamictons in a polar-marine setting. *Mar. Geol.* **216**, 191–204.

Hillenbrand C. D., Camerlenghi A., Cowan E. A., Hernández-Molina F. J., Lucchi R. G., Rebesco M. and Uenzelmann-Neben G. (2008a) The present and past bottom-current flow regime around the sediment drifts on the continental rise west of the Antarctic Peninsula. *Mar. Geol.* **255**, 55–63.

Hillenbrand C. D., Crowhurst S. J., Williams M., Hodell D. A., McCave I. N., Ehrmann W., Xuan C., Piotrowski A. M., Hernández-Molina F. J., Graham A. G. C., Grobe H., Williams T. J., Horrocks J. R., Allen C. S. and Larter R. D. (2021) New insights from multi-proxy data from the West Antarctic continental rise: Implications for dating and interpreting Late Quaternary palaeoenvironmental records. *Quat. Sci. Rev.* **257**, 106842.

Hillenbrand C. D. and Ehrmann W. (2005) Late Neogene to Quaternary environmental changes in the Antarctic Peninsula region: Evidence from drift sediments. *Glob. Planet. Change* **45**, 165–191.

Hillenbrand C. D., Ehrmann W., Larter R. D., Benetti S., Dowdeswell J. A., Ó Cofaigh C., Graham A. G. C. and Grobe H. (2009) Clay mineral provenance of sediments in the southern Bellingshausen Sea reveals drainage changes of the West Antarctic Ice Sheet during the Late Quaternary. *Mar. Geol.* **265**, 1–18.

Hillenbrand C. D., Grobe H., Diekmann B., Kuhn G. and Fütterer D. K. (2003) Distribution of clay minerals and proxies for productivity in surface sediments of the Bellingshausen and Amundsen seas (West Antarctica) - Relation to modern environmental conditions. *Mar. Geol.* **193**, 253–271.

Hillenbrand C. D., Larter R. D., Dowdeswell J. A., Ehrmann W., Ó Cofaigh C., Benetti S., Graham A. G. C. and Grobe H. (2010) The sedimentary legacy of a palaeo-ice stream on the shelf of the southern Bellingshausen Sea: Clues to West Antarctic glacial history during the Late Quaternary. *Quat. Sci. Rev.* **29**, 2741–2763.

Hillenbrand C. D., Moreton S. G., Caburlotto A., Pudsey C. J., Lucchi R. G., Smellie J. L., Benetti S., Grobe H., Hunt J. B. and Larter R. D. (2008b) Volcanic time-markers for Marine Isotopic Stages 6 and 5 in Southern Ocean sediments and Antarctic ice cores: implications for tephra correlations between palaeoclimatic records. *Quat. Sci. Rev.* **27**, 518–540.

Howe J. N. W., Piotrowski A. M., Noble T. L., Mulitza S., Chiessi C. M. and Bayon G. (2016) North Atlantic Deep Water Production during the Last Glacial Maximum. *Nat. Commun.* **7**, 1–8.

Huang H., Gutjahr M., Kuhn G., Hathorne E. C. and Eisenhauer A. (2021) Efficient extraction of past seawater Pb and Nd isotope signatures from Southern Ocean Sediments. *Geochem, Geophys. Geosyst.* **22**.

Huang T. C., Watkins N. D. and Shaw D. M. (1975) Atmospherically transported volcanic glass in deep-sea sediments: Volcanism in sub-antarctic latitudes of the South Pacific during late pliocene and pleistocene time. *GSA Bull.* **9**, 1305–1315.

Jacobsen S. B. and Wasserburg G. J. (1980) Sm-Nd isotopic evolution of chondrites. *Earth Planet. Sci. Lett.* **50**, 139–155.

Johannesson K. H. and Burdige D. J. (2007) Balancing the global oceanic neodymium budget: Evaluating the role of groundwater. *Earth Planet. Sci. Lett.* **253**, 129–142.

Kim J. H., Torres M. E., Haley B. A., Kastner M., Pohlman J. W., Riedel M. and Lee Y. J. (2012) The effect of diagenesis and fluid migration on rare earth element distribution in pore fluids of the northern Cascadia accretionary margin. *Chem. Geol.* **291**, 152–165.

Klinkhammer G. P. and Palmer M. R. (1991) Uranium in the oceans: Where it goes and why. *Geochim. Cosmochim. Acta* **55**, 1799–1806.

Koeppenkastrop D. and De Carlo E. H. (1993) Uptake of rare earth elements from solution by metal oxides. *Environ. Sci. Technol.* **27**, 1796–1802.

Ku T., Mathieu G. G. and Knauss K. G. (1977) Uranium in open ocean: Concentration and isotopic composition. *Deep Sea Res.* **24**, 1005–1017.

Lacan F. and Jeandel C. (2005) Neodymium isotopes as a new tool for quantifying exchange fluxes at the continent-ocean interface. *Earth Planet. Sci. Lett.* **232**, 245–257.

Larkin C. S., Piotrowski A. M., Hindshaw R. S., Bayon G., Hilton R. G., Jotautas B. J., Dellinger M., Wang R. and Tipper E. T. (2021) Constraints on the source of reactive phases in sediment from a major Arctic river using neodymium isotopes. *Earth Planet. Sci. Lett.* **565**, 116933.

Li Y.-H. and Gregory S. (1974) Diffusion of ions in sea water and in deep-sea sediments. *Geochim. Cosmochim. Acta* **38**, 703–714.

Li Y. (2018) *Investigating sediment size distributions and size-specific Sm-Nd isotopes as paleoceanographic proxy in the North Atlantic Ocean: Reconstructing past deep-sea current speeds since Last Glacial Maximum*. University of Cambridge), Doctoral dissertation.

Lucchi R. G., Rebesco M., Camerlenghi A., Busetti M., Tomadin L., Villa G., Persico D., Morigi C., Bonci M. C. and Giorgetti G. (2002) Mid-late pleistocene glacimarine sedimentary processes of a high-latitude, deep-sea sediment drift (Antarctic Peninsula Pacific margin). *Mar. Geol.* **189**, 343–370.

Meredith M. P. (2013) Oceanography: Replenishing the abyss. *Nat. Geosci.* **6**, 166–167.

Middelburg J. J., Soetaert K. and Herman P. M. J. (1997) Empirical relationships for use in global diagenetic models. *Deep Res. Part I Oceanogr. Res. Pap.* **44**, 327–344.

Nitsche F. O., Cunningham A. P., Larter R. D. and Gohl K. (2000) Geometry and development of glacial continental margin depositional systems in the Bellingshausen Sea. *Mar. Geol.* **162**, 277–302.

Ó Cofaigh C., Larter R. D., Dowdeswell J. A., Hillenbrand C. D., Pudsey C. J., Evans J. and Morris P. (2005) Flow of the West Antarctic Ice Sheet on the continental margin of the Bellingshausen Sea at the Last Glacial Maximum. *J. Geophys. Res. Solid Earth* **110**, 1–13.

Park Y. K., Lee J. I., Jung J., Hillenbrand C.-D., Yoo K.-C. and Kim J. (2019) Elemental compositions of smectites reveal detailed sediment provenance changes during glacial and interglacial periods: the southern Drake Passage and Bellingshausen Sea, Antarctica. *Minerals* **9**, 322.

Paul S. A. L., Haeckel M., Bau M., Bajracharya R. and Koschinsky A. (2019) Small-scale heterogeneity of trace metals including REY in deep-sea sediments and pore waters of the Peru Basin, SE equatorial Pacific. *Biogeosci. Discuss.*, 1–29.

Petschick R., Kuhn G. and Gingele F. X. (1996) Clay mineral distribution in surface sediments of the South Atlantic: sources, transport, and relation to oceanography. *Mar. Geol.* **130**, 203–229.

Pierce E. L., Williams T., Van De Flierdt T., Hemming S. R., Goldstein S. L. and Brachfeld S. A. (2011) Characterizing the sediment provenance of East Antarctica's weak underbelly: The Aurora and Wilkes sub-glacial basins. *Paleoceanography* **26**.

Piotrowski A. M., Goldstein S. L., Hemming S. R. and Fairbanks R. G. (2004) Intensification and variability of ocean thermohaline circulation through the last deglaciation. *Earth Planet. Sci. Lett.* **225**, 205–220.

Piotrowski A. M., Goldstein S. L., Hemming S. R. and Fairbanks R. G. (2005) Temporal relationship of carbon cycling and ocean circulation at glacial boundaries. *Science (80-.)* **307**, 1933–1938.

Pudsey C. J. (2000) Sedimentation on the continental rise west of the Antarctic Peninsula over the last three glacial cycles. *Mar. Geol.* **167**, 313–338.

Pudsey C. J. and Camerlenghi A. (1998) Glacial-interglacial deposition on a sediment drift on the Pacific margin of the Antarctic Peninsula. *Antarct. Sci.* **10**, 286–308.

Rebesco M., Larter R. D., Barker P. F., Camerlenghi A. and Vanneste L. E. (1997) The history of sedimentation on the continental rise west of the Antarctic Peninsula. In *Geology and Seismic Stratigraphy of the Antarctic Margin* pp. 29–49.

Rebesco M., Larter R. D., Camerlenghi A. and Barker P. F. (1996) Giant sediment drifts on the upper continental rise west of the Antarctic Peninsula. *Geo-Marine Lett.* **16**, 65–75.

Rebesco M., Pudsey C. J., Canals M., Camerlenghi A., Barker P. F., Estrada F. and Giorgetti A. (2002) Sediment drifts and deep-sea channel systems, Antarctic Peninsula Pacific Margin. *Geol. Soc. Mem.* **22**, 353–371.

Rickli J., Frank M. and Halliday A. N. (2009) The hafnium-neodymium isotopic composition of Atlantic seawater. *Earth Planet. Sci. Lett.* **280**, 118–127.

Rickli J., Gutjahr M., Vance D., Fischer-Gödde M., Hillenbrand C. D. and Kuhn G. (2014) Neodymium and hafnium boundary contributions to seawater along the West Antarctic continental margin. *Earth Planet. Sci. Lett.* **394**, 99–110.

Robinson S., Ivanovic R., van de Flierdt T., Blanchet C. L., Tachikawa K., Martin E. E., Cook C. P., Williams T., Gregoire L., Plancherel Y., Jeandel C. and Arsouze T. (2021) Global continental and marine detrital εNd: An updated compilation for use in understanding marine Nd cycling. *Chem. Geol.* **567**, 120119.

Rousseau T. C. C., Sonke J. E., Chmeleff J., Candaudap F., Lacan F., Boaventura G., Seyler P. and Jeandel C. (2013) Rare earth element analysis in natural waters by multiple isotope dilution-sector field ICP-MS. *J. Anal. At. Spectrom.* **28**, 573–584.

Roy M., van de Flierdt T., Hemming S. R. and Goldstein S. L. (2007) $^{40}Ar/^{39}Ar$ ages of hornblende grains and bulk Sm/Nd isotopes of circum-Antarctic glacio-marine sediments: Implications for sediment provenance in the southern ocean. *Chem. Geol.* **244**, 507–519.

Scheuer C., Gohl K., Larter R. D., Rebesco M. and Udintsev G. (2006) Variability in Cenozoic sedimentation along the continental rise of the Bellingshausen Sea, West Antarctica. *Mar. Geol.* **227**, 279–298.

Schnetger B. and Dellwig O. (2012) Dissolved reactive manganese at pelagic redoxclines (part I): A method for determination based on field experiments. *J. Mar. Syst.* **90**, 23–30.

Scott M. (1994) Rare earth element geochemistry and the tetrad effect. *Geochim. Cosmochim. Acta* **58**, 2025–2033.

Shane P. A. R. and Froggatt P. C. (1992) Composition of widespread volcanic glass in deep-sea sediments of the Southern Pacific Ocean: An Antarctic source inferred. *Bull. Volcanol.* **6**, 595–601.

Shaw T. J., Gieskes J. M. and Jahnke R. A. (1990) Early diagenesis in differing depositional environments: The response of transition metals in pore water. *Geochim. Cosmochim. Acta* **54**, 1233–1246.

Sholkovitz E. R., Piepgras D. J. and Jacobsen S. B. (1989) The pore water chemistry of rare earth elements in Buzzards Bay sediments. *Geochim. Cosmochim. Acta* **53**, 2847–2856.

Siddall M., Khatiwala S., van de Flierdt T., Jones K., Goldstein S. L., Hemming S. and Anderson R. F. (2008) Towards explaining the Nd paradox using reversible scavenging in an ocean general circulation model. *Earth Planet. Sci. Lett.* **274**, 448–461.

Simoes Pereira P., van de Flierdt T., Hemming S. R., Hammond S. J., Kuhn G., Brachfeld S., Doherty C. and Hillenbrand C. D. (2018) Geochemical fingerprints of glacially eroded bedrock from West Antarctica: Detrital thermochronology, radiogenic isotope systematics and trace element geochemistry in Late Holocene glacial-marine sediments. *Earth-Sci. Rev.* **182**, 204–232.

Smrzka D., Zwicker J., Bach W., Feng D., Himmler T., Chen D. and Peckmann J. (2019) *The Behavior of Trace Elements in Seawater, Sedimentary Pore Water, and Their Incorporation into Carbonate Minerals: A Review*. Springer, Berlin Heidelberg.

Soetaert K., Herman P. M. J. and Middelburg J. J. (1996) A model of early diagenetic processes from the shelf to abyssal depths. *Geochim. Cosmochim. Acta* **60**, 1019–1040.

Stichel T., Frank M., Hathorne E. C., Haley B. A., Jeandel C. and Pradoux C. (2012) Sources and input mechanisms of hafnium and neodymium in surface waters of the Atlantic sector of the Southern Ocean. *Geochim. Cosmochim. Acta* **94**, 22–37.

Stichel T., Pahnke K., Duggan B., Goldstein S. L., Hartman A. E., Paffrath R. and Scher H. D. (2018) TAG plume: Revisiting the hydrothermal neodymium contribution to seawater. *Front. Mar. Sci.* **5**, 96.

Tachikawa K., Arsouze T., Bayon G., Bory A., Colin C., Dutay J. C., Frank N., Giraud X., Gourlan A. T., Jeandel C., Lacan F., Meynadier L., Montagna P., Piotrowski A. M., Plancherel Y., Pucéat E., Roy-Barman M. and Waelbroeck C. (2017) The large-scale evolution of neodymium isotopic composition in the global modern and Holocene ocean revealed from seawater and archive data. *Chem. Geol.* **457**, 131–148.

Tachikawa K., Athias V. and Jeandel C. (2003) Neodymium budget in the modern ocean and paleo-oceanographic implications. *J. Geophys. Res. C Ocean.* **108**, 10–11.

Tanaka T., Togashi S., Kamioka H., Amakawa H., Kagami H., Hamamoto T., Yuhara M., Orihashi Y., Yoneda S., Shimizu H., Kunimaru T., Takahashi K., Yanagi T., Nakano T., Fujimaki H., Shinjo R., Asahara Y., Tanimizu M. and Dragusanu C. (2000) JNdi-1: A neodymium isotopic reference in consistency with LaJolla neodymium. *Chem. Geol.* **168**, 279–281.

Taylor S. R. and McLennan S. M. (1985) The continental crust: Its composition and evolution.

Tucholke B. E. (1977) Sedimentation processes and acoustic stratigraphy in the Bellingshausen Basin. *Mar. Geol.* **25**, 209–230.

Ullman W. J. and Aller R. C. (1982) Diffusion coefficients in nearshore marine sediments1. *Limnol. Oceanogr.* **27**, 552–556.

Volpi V., Camerlenghi A., Hillenbrand C. D., Rebesco M. and Ivaldi R. (2003) Effects of biogenic silica on sediment compaction and slope stability on the Pacific margin of the Antarctic Peninsula. *Basin Research* **15**(3), 339–363.

Walter H. J., Hegner E., Diekmann B., Kuhn G. and Rutgers Van Der Loeff M. M. (2000) Provenance and transport of terrigenous sediment in the South Atlantic Ocean and their relations to glacial and interglacial cycles: Nd and Sr isotopic evidence. *Geochim. Cosmochim. Acta* **64**, 3813–3827.

Wang R., Clegg J. A., Scott P. M., Larkin C. S., Deng F., Thomas A. L., Zheng X.-Y. and Piotrowski A. M. (2021) Reversible scavenging and advection–Resolving the neodymium paradox in the South Atlantic. *Geochim. Cosmochim. Acta* **314**, 121–139.

Wilson D. J., Bertram R. A., Needham E. F., van de Flierdt T., Welsh K. J., McKay R. M., Mazumder A., Riesselman C. R., Jimenez-Espejo F. J. and Escutia C. (2018) Ice loss from the East Antarctic Ice Sheet during late Pleistocene interglacials. *Nature* **561**, 383–386.

Wilson D. J., Piotrowski A. M., Galy A. and Clegg J. A. (2013) Reactivity of neodymium carriers in deep sea sediments : Implications for boundary exchange and paleoceanography. *Geochim. Cosmochim. Acta* **109**, 197–221.

Wilson D. J., Piotrowski A. M., Galy A. and Mccave I. N. (2012) A boundary exchange influence on deglacial neodymium isotope records from the deep western Indian Ocean. *Earth Planet. Sci. Lett.* **341–344**, 35–47.

Wu S., Kuhn G., Diekmann B., Lembke-Jene L., Tiedemann R., Zheng X., Ehrhardt S., Arz H. W. and Lamy F. (2019) Surface sediment characteristics related to provenance and ocean circulation in the Drake Passage sector of the Southern Ocean. *Deep. Res. Part I Oceanogr. Res. Pap.* **154**, 103135.

Associate editor: Franco Marcantonio